Critical role of somatostatin receptor 2 in the vulnerability of the central noradrenergic system: new aspects on Alzheimer's disease

Csaba Ádori - Laura Glück - Swapnali Barde - Takashi Yoshitake - Gabor G. Kovacs - Jan Mulder - Zsófia Maglóczky - László Havas - Kata Bölcskei - Nicholas Mitsios - Mathias Uhlén - János Szolcsányi - Jan Kehr - Annica Rönnbäck - Thue Schwartz - Jens F. Rehfeld - Tibor Harkany - Miklós Palkovits - Stefan Schulz - Tomas Hökfelt

C. Adori – S. Barde – J. Mulder – N. Mitsios – T. Hökfelt
Department of Neuroscience, Karolinska Institutet, SE-17177, Stockholm, Sweden

L. Glück – S. Schultz
Institute of Pharmacology and Toxicology, Jena University Hospital, Friedrich-Schiller University, D-07747, Jena, Germany

T. Yoshitake – J. Kehr
Department of Physiology and Pharmacology, Karolinska Institutet, SE-17177, Stockholm, Sweden

G. G. Kovacs
Institute of Neurology, Medical University of Vienna, A-1097, Vienna, Austria

J. Mulder – N. Mitsios
Science for Life Laboratory, Karolinska Institutet, SE-17177, Stockholm, Sweden

Z. Maglóczky
Laboratory of Cerebral Cortex Research, Institute of Experimental Medicine of the Hungarian Academy of Sciences, H-1083, Budapest, Hungary

L. Havas
Department of Pathology, Szent Borbála Hospital, H-2800, Tatabánya, Hungary

K. Bölcskei – J. Szolcsányi Department of Pharmacology and Pharmacotherapy, University of Pécs Medical School, H-7624, Pécs Hungary

M. Uhlén
Science for Life Laboratory, Royal Institute of Technology, SE-10691, Stockholm, Sweden

A. Rönnbäck
Department of Neurobiology, Care Sciences and Society, Karolinska Institutet Alzheimer Disease Research Center, Center for Alzheimer Research, Division for Neurogeriatrics, Karolinska Institutet, SE-14157, Stockholm, Sweden

T. Schwartz
Novo Nordisk Foundation Center for Basic Metabolic Research, Section for Metabolic Receptology and Enteroendocrinology, and Laboratory for Molecular Pharmacology, Department of Neuroscience and Pharmacology, University of Copenhagen, DK-2200, Copenhagen, Denmark

J. F. Rehfeld
Department of Clinical Biochemistry, Rigshospitalet, University of Copenhagen, DK-2500, Copenhagen, Denmark

T. Harkany
Department of Medical Biochemistry and Biophysics, Karolinska Institutet, SE-17177, Stockholm, Sweden and
Department of Molecular Neurosciences, Center for Brain Research, Medical University of Vienna, A-1090, Vienna, Austria

M. Palkovits
Neuromorphological and Neuroendocrine Research Laboratory, Department of Anatomy, Histology and Embryology, Semmelweis University and the Hungarian Academy of Sciences, Budapest, Hungary and Human Brain Tissue Bank and Laboratory, Semmelweis University, H-1085, Budapest, Hungary

Corresponding authors *Csaba Adori PhD*, Department of Neuroscience, Retzius Laboratory, Karolinska Institutet, Retzius väg 8, 17177 Stockholm, Sweden, E-mail: csaba.adori@ki.se, telephone: +46 8 52487097, Fax: +46 8 331692 and *Tomas Hökfelt MD PhD*, Department of Neuroscience, Retzius Laboratory, Karolinska Institutet, Retzius väg 8, 17177 Stockholm, Sweden, E-mail: tomas.hokfelt@ki.se, telephone: +46 8 52487070, Fax: +46 8 331692

Abstract Alzheimer's disease and other age-related neurodegenerative disorders are associated with deterioration of the noradrenergic locus coeruleus (LC), a probable trigger for mood and memory dysfunction. LC noradrenergic neurons exhibit particularly high levels of somatostatin binding sites. This is noteworthy since cortical and hypothalamic somatostatin content is reduced in neurodegenerative pathologies. Yet the role of a somatostatin signal-deficit in the maintenance of noradrenergic projections remains unknown. Here, we deployed tissue microarrays, immunohistochemistry, quantitative morphometry and mRNA profiling in a cohort of Alzheimer's and age-matched control brains in combination with genetic models of somatostatin receptor deficiency to establish causality between defunct somatostatin signalling and noradrenergic neurodegeneration. In Alzheimer's disease, we found significantly reduced somatostatin protein expression in the temporal cortex, with aberrant clustering and bulging of tyrosine hydroxylase-immunoreactive afferents. As such, somatostatin receptor 2 (SSTR2) mRNA was highly expressed in the human LC, with its levels significantly decreasing from Braak stages III/IV and onwards, i.e. a process preceding advanced Alzheimer's pathology. The loss of *SSTR2* transcripts in the LC neurons was selective, since tyrosine hydroxylase, dopamine ß-hydroxylase, galanin or galanin receptor 3 mRNAs remained unchanged. We modeled these pathogenic changes in *Sstr2*$^{-/-}$ mice and, unlike in *Sstr1*$^{-/-}$ or *Sstr4*$^{-/-}$ genotypes, they showed selective, global and progressive degeneration of their central noradrenergic projections. However, neuronal perikarya in the LC were found intact until late adulthood (<8 months) in *Sstr2*$^{-/-}$ mice. In contrast, the noradrenergic neurons in the superior cervical ganglion lacked SSTR2 and, as expected, the sympathetic innervation of the head region did not show any signs of degeneration. Our results indicate that SSTR2-mediated signaling is integral to the maintenance of central noradrenergic projections at the system level, and that early loss of somatostatin receptor 2

function may be associated with the selective vulnerability of the noradrenergic system in Alzheimer's disease.

Keywords: neuropeptide – co-existence – Alzheimer's disease – depression – noradrenaline – somatostatin receptor

Supplementary material This manuscript contains one supplementary material file

Introduction

Locus coeruleus (LC) is a key node in the mammalian brain sending projections to virtually all parts of the central nervous system [8,40,72,47]. Its principle transmitter is noradrenaline (NA) [26]. The NA circuitry is involved in multiple physiological processes, including arousal, wakefulness, memory and motor functions as well as stress and mood regulation [39,9,18,73,17,11,97]. Several clinical studies indicate degenerative changes of the central noradrenergic system in Alzheimer's disease [12,22,44,65,103] as well as in Parkinson's disease and in Down's syndrome [44]. Impairment of this monoamine system is also involved in major depressive disorder [93,18]. In fact, in Alzheimer's disease neuronal loss is more pronounced in LC than in the nucleus basalis of Meynert [119]. Recently, pre-tangle formation was found in the LC of young individuals, supporting the hypothesis that LC/subcoeruleus represents an early starting point for Alzheimer's disease pathology, even preceding the occurrence of cortical lesions [10,13,15]. Nevertheless, the cause(s) and underlying mechanism(s) of the early LC degeneration in Alzheimer's disease remain unclear.

In addition to direct functional deficits, NA lesions may induce amyloid formation via microglial inflammatory processes [52] and via loss of BDNF production or brain microvascular impairments [48,85]. The currently used mouse models of Alzheimer's disease (transgenic mice expressing mutant forms of amyloid precursor protein (APP), presenilins and tau, singly or in combination), however, exhibit at most mild LC degeneration or no degeneration at all [115,45]. In contrast, a selective. chemical lesion of LC in APP-mutant mice induced by DSP4 (N-(2-chloroethyl)-N-ethyl-2-bromobenzylamine hydrochloride) exacerbates the Aβ plaque load as well as cholinergic and spatial memory deficits [49,115]. Also, when *Ear2*$^{-/-}$ mice with an early noradrenergic deficit (Ear2 is an orphan nuclear receptor necessary for the development of LC neurons in mice) were crossed with APP/PS1 mice, they exhibited a significantly more severe impairment of spatial memory and

hippocampal long-term potentiation than mice with either APP/PS1 mutation or loss of Ear2 alone [60]. Thus, these transgenic animal models are useful tools to study the consequences of noradrenergic impairment in experimental models of Alzheimer's disease but lack the inherent capacity to reveal candidate mechanism(s) underlying LC vulnerability.

Another, early established neurochemical hallmark of Alzheimer's disease is a substantial deficit of somatostatin (SST) in cortical areas and in the hypothalamus [20,76,27,58,89]. SST is a regulatory peptide originally discovered as the hypothalamic factor inhibiting growth hormone release [16,107] and subsequently found to have wide distribution and multiple functions in the brain [34,112]. SST acts via six subtypes of G-protein-coupled receptors, of which SSTR2(a) is one of the most abundant in the brain [54,112,101]. In Alzheimer's disease SST was the most consistently reduced among all neuropeptides so far examined [20]. Likewise, *SSTR2* mRNA expression was significantly decreased in the frontal and temporal cortices [42,59]. Amyloid plaques show immunoreactivity for SST [74]. Also, polymorphisms of the *SST* gene are risks factors for Alzheimer's disease [111,117], albeit not confirmed in genome-wide association studies (GWAS). SST regulates the metabolism of Aβ through increasing neprylisin activity [90]. SST deficits were also detected in major depressive- and bipolar disorders [64]. Moreover, SSTR2/SSTR3 modulation of monoamine systems may induce antidepressant effects in rats [32,33]. Results on SST impairments in Alzheimer's disease mouse models are not consistent [53,91]. However, one study on APPxPS1 mice reported an early decrease of *SST* expression and selective loss of SST-expressing interneurons in the hippocampus [84], which was also described in human post mortem samples [58,27]. These observations could provide explanations for the intimate correlation of the decrease in SST levels and cognitive deficit in Alzheimer's disease [36].

Interestingly, the density of SST binding sites is very high in the LC both in the rodent [35,41] and human brain [21], and SST has strong inhibitory effect on LC neurons in vitro

[68,79,55,23] and in vivo [104]. However, less attention has been paid to a potential contribution of the well-established SST impairment to the well-defined noradrenergic deficit in neurodegenerative disorders.

To fill this gap, we first examined the expression of *SSTR2* in LC samples from Alzheimer's disease cases and age-matched control subjects and found a decrease already in individuals with intermediate Alzheimer's disease neuropathological changes, Braak III-IV stage. Then we studied the potential role of SST receptors in the maintenance of the noradrenergic system in transgenic animal strains. Thus, the morphology and neurochemistry of neurocircuitries were examined in *Sstr1*, *Sstr2* and *Sstr4* knockout animals with special attention to the monoaminergic systems. We show that the deletion of *Sstr2*, but not the other two SST receptors, results in a selective, global and progressive noradrenergic axonal degeneration.

Materials and experimental procedures

Detailed descriptions of human brains, *Sstr* knockout/LacZ-knockin mice strains and methods are provided in the Supplementary Information (SI).

Immunohistochemistry on perfused human brains

Human brains (N = 2; Suppl. Table 1) were obtained from the Department of Pathology, Szent Borbála Hospital, Tatabánya, Hungary. All procedures were approved by the Regional and Institutional Committee of Science and Research Ethics of Scientific Council of Health (ETT TUKEB 31443/2011/EKU, 518/PI/11, Hungary) and were in agreement with the Declaration of Helsinki.

Brains were removed 4 hours after death. Both internal carotid and vertebral arteries were cannulated, the brains were perfused as described [105]. Double-immunostaining procedure, confocal analysis and micrograph production were performed as described for animal tissue.

Quantitative PCR on human LC micro-punch samples

Pieces of frozen human brainstems were obtained from the Human Tissue Bank, Semmelweis University, Hungary (HBTB, ethical permission numbers: 6008/8/2002/ETT and 32/1992/TUKEB). HBTB is a member of the BrainNet II Europe consortium. Procedures were in agreement with the Declaration of Helsinki. Neuropathological and histochemical examination of all brains, including classification of amyloid-β plaque burden, tau pathology and synuclein pathology was performed as described in the SI. Brains with Alzheimer's disease Braak stage V-VI (N=7), with intermediate Alzheimer's disease neuropathologic changes (Braak stage III-IV) (N=5) and age-matched controls with no neurodegenerative alterations and with no signs of clinical neuropsychiatric disease (N=9) were selected (Suppl. Table 2).

During the micro-punch procedure, 1.0-1.5 mm thick coronal sections were cut at the level of LC and 4-6 tissue pellets were collected bilaterally with the application of 0.7 mm inside diameter microdissection needles (two from each coronal section) and kept frozen at minus 70^{o}C pending analysis.

Total RNA from punched LC samples was extracted using the RNeasy Mini kit (Qiagen, Sollentuna, Sweden). TaqMan assay for tyrosine hydroxylase (TH (Hs00165941_m1) was purchased from Applied Biosystems (Carlsbad, CA) and the amplification reaction was carried out using TaqMan assay master mix (Applied Biosystems). All other primers were purchased from Sigma-Aldrich (Suppl. Table 3). Gene expression was

measured by quantitative reverse transcription polymerase chain reaction (qRT-PCR) on an Applied Biosystems 7000 Real-Time PCR system. Relative fold changes were calculated by using the comparative CT method ($2^{-\Delta\Delta CT}$).

Tissue microarray (TMA) on human samples

Formalin fixed brains were obtained from the Dutch Brain Bank (NBB, ethical permission no. EPN 2013/474-31/2). Procedures were in agreement with the Declaration of Helsinki. Detailed neuropathological examination of all brains was performed as described in the SI.

A TMA block containing temporal cortex samples from Alzheimer's disease subjects (N=7, Braak stage VI) and 9 age-matched controls (Suppl. Table 4) was constructed [56]. TMA slides were triple stained sequentially on a BOND-RX autostainer (Leica Microsystems, Wetzlar, Germany) for tyrosine hydroxylase (TH) or SST, amyloid-β and tau-PHF using tyramide signal amplification (TSA) method [1]. Slides were scanned on the VSlide scanning system (Metasystems, Alltlussheim, Germany) using 20x objectives and appropriate filter sets. Immunostaining for SST, amyloid-β and tau-PHF was quantified by densitometry with the Image J 1.37v software (1.37v, NIH, MD).

Transgenic animals

Experiments were performed on (i) 2-week and 1-, 2-, 4- and 8-month-old male homozygote *Sstr2* knockout/LacZ knockin mice (*Sstr2*$^{-/-}$) [5,6], (ii) 4-month-old male homozygote *Sstr1* knockout/LacZ knockin mice (*Sstr1*$^{-/-}$) [61], (iii) 8-month-old male *Sstr4* knockout/LacZ knockin mice (*Sstr4*$^{-/-}$) [51] and on three 15-month-old male homozygous TgAPParc transgenic mice and on their wild-type littermates (*WT*s) [87,88]. Experimental procedures were approved by the local ethical committee (Stockholms norra djurförsöksetiska nämnd, N171-172/11), and conformed to the European Communities Council Directive #86/609/EEC and the "Principles of laboratory animal care" (NIH publication No. 86-23, revised 1985).

Particular care was taken to minimize the number of animals and their suffering throughout the experiments.

Fluorescence immunohistochemistry and microscopy/confocal analysis of mice

Mice were transcardially perfused with Zamboni fixative [28]. Sections were incubated overnight with primary antibodies (Table S5A) and processed using a commercial immunostaining kit (PerkinElmer Life Science, Boston, MA) based on tyramide signal amplification [1]. Numerous immunostained sections were sequentially double-stained with additional antibodies (Suppl. Table 5a–b) and examined with a Zeiss LSM 510 Meta confocal-system installed on a Zeiss Axioplan 2 microscope.

Morphometry

Cell body counting and determination of mean somatic surface area

For each animal (8-month-old, N=3), 4 sections, immunostained for TH, counterstained with nuclear marker TO-PRO®-3, were analyzed at four different rostro-caudal levels of the LC. The number of TH-positive$^{(+)}$ cells/mm^2 and somatic surface area of each neuron (μm^2/cell) were measured using the Image J 1.37v software. Altogether 1,014 cells from *Sstr2*$^{-/-}$ (338±93/animal) and 989 cells (329±10/animal) from *WT* were examined.

Densitometry of TH$^+$ fibers and counting of enlarged varicosities and fiber clusters

Mouse brain coronal sections (Bregma -5 to -4) from two-week, 1-, 2-, 4- and 8-month-old *WT* and *Sstr2*$^{-/-}$ animals (N=3-5), immunostained for TH, were captured on a *Vslide* scanning microscope (Metasystems). The number of 'single swollen varicosities/intervaricose connections' and 'aberrant fiber clusters'/mm^2 were determined in unilateral fronto-parietal cortices as described before [3]. A detailed description of these aberrant structures is reported in the Results and Fig. 7, Suppl. Fig. 2, legends). To determine the TH$^+$ fiber density, we applied a 1-pixel algorithm using the Image J 1.37v in micrographs.

Semiquantitative score of aberrant noradrenergic structures

A four-grade score was applied at numerous rostro-caudal levels (Table 1, legend) of three 4-month- and three 8-month-old brains [immunostained for the NA/norepinephrine transporter (NET)].

Quantitative in situ hybridization (qISH)

Mice (4-month-old, N=5/genotype) were decapitated and the brains rapidly dissected and snap-frozen. Antisense oligoprobes (TH, galanin), complementary or highly homologous to the mouse mRNA sequence, were synthesized by CyberGene AB (Huddinge, Sweden). The oligonucleotides were radioactively labeled with ^{33}P, and sections were hybridized as described [92] and dipped in Kodak NTB-2 emulsion (Kodak, Rochester, NY). The transcript levels for TH and galanin expression in LC were quantified using an image analysis system (see SI). The number of silver grains was measured over the cell bodies with the Image J 1.37v software.

HPLC measurement of monoamines

Mice (2-week and 4-month-old, N=5/genotype) were decapitated and fronto-parietal cortex, caudate-putamen and dorsal hippocampus samples were dissected and homogenized. Concentrations of NA, dopamine (DA), serotonin (5-hydroxytryptamine, 5-HT) were determined by HPLC as described [57]. The chromatograms were recorded and integrated by use of the computerized data acquisition system Clarity (DataApex, Prag, Czeck Republic).

Statistical analyses

One-way ANOVA and Fisher post-hoc tests were applied for human qPCR studies. Student's t-test for independent samples was applied for the evaluation of densitometry on human TMA slides. One- and two-way ANOVA (quantification of aberrant fiber structures, fiber density measurements, respectively) and Tukey's post-hoc test; three-way ANOVA and Tukey-test (HPLC measurements) and Student's t-test for independent samples (qISH, cell body or somatic surface area, HPLC) were applied for animal studies. All data were evaluated with

acceptable levels of significance set at $P < 0.05$ using Statistica® 7 software. All variables, numerical data of ANOVA F/df and main effect P values are reported in Suppl. Tables 6-7.

Results

Somatodendritic localization of SSTR2a in the human LC

To determine the precise localization of SSTR2 in the LC region, perfused non-neurodegenerative human brainstems were studied. Prominent somatodendritic SSTR2a localization was found in many LC noradrenergic (TH-immunoreactive, IR) neurons in both examined human brainstems but not in other nuclei at the level of LC (Fig. 1a–d).

Decreased *SSTR2* expression in the LC of Alzheimer's subjects

In order to determine the expression-level of *SSTR2*, micro-punch samples from the LC were collected from verified Braak III-IV and V-VI stage subjects and age-matched controls (Suppl. Table 2). *SSTR2* mRNA expression-levels were high in controls, compared to those of galanin (*GAL*) or galanin receptor 3 (*GALR3*), members of another inhibitory neuropeptide system in LC neurons (Fig. 2a; a higher Ct value reflects a lower expression-level).

SSTR2 expression significantly decreased in both Braak III-IV (-48%) and Braak V-VI (-45%) groups compared to the age-matched controls. The transcripts for neuron-specific microtubule associated protein (*MAP2*) also decreased significantly in the Braak III-IV group (-68%) but, interestingly, its expression-level was improved in the Braak V-VI group (Fig. 2b). *SSTR2* and *MAP2* expressions did not correlate with age, gender or post mortem delay (PMD) (data not shown).

No significant changes in transcript levels for *TH*, the rate-limiting enzyme of noradrenaline synthesis, *dopamine β-hydroxylase* (*DBH*), *GAL* or *GALR3* were noted in either Alzheimer's groups, compared to age-matched controls. However, a trend towards increase both in *TH* and *GALR3* (Fig. 2b) expression was found in the Braak III-IV group.

Relative fold-changes for *SSTR2* gene expression levels were normalized to *β-III-tubulin* (*TUBB3*) as well as to *β-ACTIN* and *GAPDH* with similar results (Fig. 2c, Suppl. Table 7).

Decreased SST immunostaining and aberrant TH-IR fibers in the temporal cortex of Alzheimer´s subjects

Next, we examined the SST immunostaining and the morphology of TH-IR fibers in the human brain, with the application of the tissue micro-array (TMA) technique (Fig. 3a). In the Alzheimer subjects (Braak V-VI, N=7), dystrophic neurites and neurofibrillary tangles were immunostained for tau-PHF throughout the TMA temporal cortex samples and senile plaques were stained for amyloid-β (Fig. 4d, g). In contrast, no amyloid-β or tau-PHF staining was noted in the controls (with a single exception for amyloid-β) (Fig. 4).

In control samples, a dense network of SST-IR processes was strongly immunostained (Fig. 4a–b), which was significantly decreased in the Alzheimer's samples (Fig. 4c–d, g), in agreement with previous reports [76].

In both control and Alzheimer's samples, rare varicose TH-IR fibers with normal morphology were immunostained (Fig. 3b–c). In samples from 3 of 10 Alzheimer's subjects, occasional clusters of aberrant TH-IR fiber structures were noted (Fig. 3d–g). These clusters were 50-100 μm in diameter, contained loose conglomerates of enlarged-swollen varicosities

(Fig. 3e, g), were negative for tau-PHF (Fig. 3d, f) and unrelated to the location of amyloid plaques (Fig.3d, f).

Noradrenergic but not dopaminergic, serotonergic or cholinergic neurons express SSTR2a in mouse

Further experiments were carried out on different *Sstr* knockout mouse strains and their wild-type littermates (Suppl. Fig. 1). First, we examined the SSTR2 protein expression of various monoaminergic and cholinergic neuron populations. A strong somatodendritic SSTR2a staining was seen in the LC and all other examined NA cell groups in *Sstr2*$^{+/+}$ (*WT*) animals (A1, A2, A6-LC, A6r and A7; see [26]) (Fig.5a–b), in agreement with a strong ß-galactosidase immunostaining (sstr2^{lacZ} staining) in the LC neurons of *Sstr2*$^{-/-}$ (knockout) mice (Fig. 5c, upper panel). Importantly, sstr1^{lacZ} or sstr4^{lacZ} staining was never found in the LC NA neurons (Fig. 5c, medial, lower panels, respectively). Moreover, serotonergic, dopaminergic or cholinergic neurons did not show co-localization with SSTR2a (Fig. 5d).

Selective noradrenergic axonal degeneration in *Sstr2*$^{-/-}$ animals

In Alzheimer's disease the noradrenergic system shows a marked vulnerability. *SSTR2/Sstr2* is highly expressed in the noradrenergic LC neurons both in human and mouse, and we found an early decrease in *SSTR2* expression in LC of Alzheimer's subjects. We therefore examined the morphology of the noradrenergic projections of *Sstr2*$^{-/-}$ mice.

The density of fibers positive for NET, DBH and, in many regions also for TH, was reduced in 4-month-old *Sstr2*$^{-/-}$ but not in *Sstr1*$^{-/-}$ or *Sstr4*$^{-/-}$ animals (Fig. 6a, c, d). In addition, swollen NET^{+}, DBH^{+} or TH^{+} fibers and sometimes large aberrant fiber clusters could be detected, exclusively in *Sstr2*$^{-/-}$ animals (Figs. 6a–d, 7, Suppl. Fig. 2 and legends). The fiber clusters intermingled with hypertrophic microglial or astroglial cells (Fig. 6b); they co-localized galanin (Fig. 6c) but were not immunoreactive for β-amyloid (Suppl. Fig. 3).

However, morphology and density of fiber networks positive for tryptophan hydroxylase-2 (TPH2), the dopamine transporter (DAT) or choline acetyltransferase (ChAT) appeared normal (Fig. 6d).

Decreased NA levels in the *Sstr2*$^{-/-}$ animals

To validate our morphological data, we then measured levels of monoamines and their main metabolites in *Sstr2*$^{-/-}$ and *WT* mice. Indeed, NA levels were significantly decreased in the fronto-parietal cortex and hippocampus but not in the striatum at 4 months-of-age. In contrast, there was no decrease in DA or serotonin levels in any region. At 2 weeks-of-age, NA levels were decreased in the hippocampus but not in fronto-parietal cortex or striatum. Serotonin levels were not altered at 2 weeks-of-age, but striatal DA levels were slightly increased (Fig. 6e).

Morphological, temporal and spatial characterization of noradrenergic axonal degeneration in *Sstr2*$^{-/-}$ mice

Next, we morphologically and quantitatively/semiquantitatively analyzed the noradrenergic degeneration in our knockout model. Fiber aberrations were divided into two categories: single swollen varicosities/intervaricose connections and dense clustering of aberrant/degenerating fibers (fiber clusters) (Fig. 7 and Suppl. Fig. 2). The single swollen varicosities/intervaricose connections were usually 5-7 μm in diameter and exhibited dense staining compared with neighboring normal noradrenergic fibers (Fig. 7e*, 7g vs. 7h, Suppl. Fig. 2a vs. 2b–c). The knot-like fiber clusters comprised aggregated, irregular-shaped, tortuous fibers with a high number of concentrated swollen varicosities/intervaricose connections. These clusters were distinct and appeared as an interruption of the adjacent normal fiber pattern. Their size varied approximately from 50 to 250 μm (Figs. 7f–f*, 6i–j, Suppl. Fig. 2d–k).

Already 1 month postnatally, the TH-IR fiber density in the fronto-parietal cortex was significantly decreased compared to the age-matched wild-type mice, and decreased further with age (Figs. 7a, 7d–f). However, single, swollen varicosities were apparent already at 2 weeks-of-age, reaching a maximum at 4 months-of-age and then gradually disappearing (Fig. 7b). In parallel, aberrant fiber clusters steadily increased until 8 months-of-age (Fig. 7c).

Signs of degeneration appeared globally in the *Sstr2*$^{-/-}$ brains, extending from the olfactory bulb to the brainstem, being most severe in neocortex, thalamus, amygdala and hippocampus. Hypothalamus, the septal region and certain brainstem areas were clearly less affected (Table 1). The decrease of NA terminals was also seen in the lumbar spinal cord, especially in the dorsal horn, but no aberrant fiber clusters could be detected here (Fig. 8a–b).

Noradrenergic LC cell bodies do not degenerate in *Sstr*$^{-/-}$ mice

Then, we examined the integrity of LC perikarya to investigate whether the noradrenergic degeneration also affected the cell bodies. The number of TH-IR cell bodies and their average soma size were not altered in 8-month-old *Sstr2*$^{-/-}$ mice compared to wild-type littermates (Fig. 9a–d). However, TH mRNA levels in the LC were modestly decreased already at 4 months-of-age (Fig. 9e–g). The expression of the modulatory neuropeptide galanin did not change significantly (Fig. 9h).

Peripheral noradrenergic nerves do not show signs of degeneration

In order to investigate whether degeneration also affects the peripheral nervous system, we examined some peripheral organs well known for a high density of noradrenergic innervation. However, NET immunostaining of salivary gland and jejunum samples did not show any sign of NA denervation or axonal degeneration (Fig. 10d–f). In agreement, only very few neurons exhibited a weak/moderate SSTR2a immunostaining in the superior cervical ganglion, the

main source of noradrenergic innervations of peripheral organs in the head region (Figure 10a–c).

Discussion

In Alzheimer's and other neurodegenerative disorders there is a serious noradrenergic impairment, including an early and marked degeneration of LC neurons. In the present study we show expression of SST receptor subtype-2 protein in noradrenergic LC neurons of control human brains, as well as a decrease in levels of its transcript already in the early stage of Alzheimer's disease. Also, the deletion of this single receptor in a mouse model causes an early-onset, global, selective and progressive noradrenergic axonal degeneration, most distinctly associated with projections from the LC. Serotonergic, dopaminergic and cholinergic fibers, however, do not degenerate. This selectivity of impairment for the noradrenergic system is confirmed by biochemical analyses. Remarkably, all NA cell groups examined, but no 5-HT, DA or cholinergic neurons, express the SST subtype-2 receptor. Additional discussion notes are provided in the SI (indicated as '*SI-D1-3*' in the following).

Decreased *SSTR2* expression in LC in Alzheimer's disease

The density of SST binding sites in the LC is very high, both in the human and rodent brain [21]. In agreement, we here show a high mRNA expression level of *SSTR2* and a strong somatodendritic immunostaining for SSTR2 protein in the human LC. *SSTR2* expression was, however, significantly decreased already in the early stages of neurodegeneration (with intermediate Alzheimer's disease neuropathological changes, Braak stage III/IV), when cognitive impairment but yet no dementia of patients occurs [75]. The LC neurons themselves do not express SST, the peptide [67]. According to early experimental studies, the SST innervation of LC mainly originates in the hypothalamus [80], where the SST levels are also

decreased in Alzheimer's subjects, as they are in many cortical regions [76,108]. These findings suggest impairment also of the LC-SST system in Alzheimer's disease. In contrast, another inhibitory neuropeptide receptor expressed in the human LC, the GALR3 [62], showed even a trend to increase in mRNA concentration in the Braak III-IV stage. The expression of *MAP2*, a dendrite- and soma-specific microtubule associated protein [83] decreased in Braak III-IV samples, as expected. However and interestingly, no change in *MAP2* expression was noted in the Braak V-VI stage, compared to control, which supports a previous report on dendritic spouting of remaining LC neurons in the terminal phase of Alzheimer's disease [99]. mRNA expression of TH, the rate limiting enzyme of NA synthesis, and of *DBH* did not decrease, in agreement with previous studies [70,99].

Interestingly, LC cell death is either very limited or nonexistent in transgenic mice models of Alzheimer's disease [115]. Thus, in the next part of our study we applied knockout mice for different SST receptors (SSTR1, 2, 4) and their wild-type littermates, to further study a potential role of SSTR2 signalling in the maintenance of the noradrenergic system. We show that *Sstr2* is expressed at high levels in all examined noradrenergic nuclei, including LC, and also in neocortical areas, while *Sstr1* and *Sstr4* are expressed in the mouse cortex but not in the LC.

Selective noradrenergic axonal degeneration in *Sstr2*$^{-/-}$ brains

The noradrenergic degeneration in *Sstr2*$^{-/-}$ mice was investigated using immunostainings for three noradrenergic markers (TH, NET, DBH), and galanin [100], the latter a neuropeptide expressed in LC neurons [71]. In contrast, no degenerative features in serotonergic, dopaminergic or cholinergic fibers were found, further underlining the selectivity of this degenerative process for the noradrenergic system, also supported by the HPLC regional measurements of NA, 5-HT and DA.

All three noradrenergic markers showed enlarged/swollen varicosities/intervaricose connections and clusters of aberrant fibers, in parallel with a substantial decrease of fiber densities. Such features have already been reported for serotonergic and cholinergic systems in normal, aging rats [7,110,77,3], as well as in the entire monoaminergic system of Zitter mutant or microenchephalic rats [106,114]. Enlarged/swollen varicosities are generated by accumulations of intra-axonal materials as a result of impaired axonal transport due to destabilization of microtubules. The knot-like fiber clusters are formed following the gradual degeneration of intervaricose connections [110,109,4].

The noradrenergic, axonal degeneration in *Sstr2*$^{-/-}$ animals is global, starts early and gradually progresses with the first distinct appearance of enlarged varicosities at around 2 weeks-of-age, followed by a gradual cluster formation from 2 months-of-age (*SI-D1*). The decrease of NA levels in general parallels the loss of noradrenergic terminals (*SI-D2*). However, the LC cell bodies seem morphologically preserved with only a modest decrease of TH mRNA levels, in any case up till 8 months-of-age, suggesting that the degeneration in *Sstr2*$^{-/-}$ animals primarily affects the axons. However, there was no evidence for degenerative processes in the peripheral noradrenergic sympathetic nerves/axons [78], nor in dopaminergic, serotonergic or cholinergic neurons, which all lacked SSTR2 immunostaining, except for a few cells in the superior cervical ganglion. Neither was degeneration detected in the noradrenergic projections of *Sstr1*$^{-/-}$ and *Sstr4*$^{-/-}$ mice, and sstr1^{LacZ} or sstr4^{LacZ} staining, respectively, was never found in the brainstem NA cells of these knockouts.

Possible mechanisms underlying the noradrenergic axonal degeneration in *Sstr2*$^{-/-}$ mice

Disturbed development/trophism

There is evidence that SST has trophic effects on neurite outgrowth [38,37]**.** Our previous results on dorsal root ganglia indicate that a SST-SSTR2a complex can be retrogradely

transported [95], perhaps mediating intracellular, trophic effects in a similar way as nerve growth factor (NGF) [63]. Thus, one explanation might be that absence of SSTR2 prevents retrograde transport of SST required for proper maintenance and development of intact NA axons and nerve terminals.

Attenuated somatodendritic inhibition and dysfunctional stress axis

SST receptors dampen the stress system [96], of which the LC is an important node (see Introduction). ACTH levels were previously found to be increased in *Sstr2* knockouts [113]. The LC neurons express *Sstr2* at high levels from the embryonic age till adulthood [101], and the postsynaptic SSTR2 mediates a strong inhibitory action of SST on spontaneous firing of LC neurons [23]. Our results confirm that LC neurons and all examined NA cell groups express a strong somatodendritic but no detectable axonal SSTR2 immunostaining postnatally in mouse; and these are the neuron groups associated with axonal degeneration. We hypothesize that the chronic absence of somatodendritic SSTR2-mediated inhibition of NA neurons leads to a continuous overexcitation and a slow, selective degeneration/accelerated aging of noradrenergic axons due to oxidative stress.

Aberrant TH-IR fibers in the temporal cortex of Alzheimer´s subjects

Despite the well-established neuronal cell body loss in LC, we do not know of any comprehensive studies on the morphology of noradrenergic axonal arborization in Alzheimer's disease. Nevertheless, NA levels [2,81] and DBH activitity [25] are decreased in Alzheimer's frontal-temporal cortical samples, supporting loss of NA fibers.

Using TMA slides, we showed clusters of apparently aberrant TH-IR fibers with enlarged varicosities from some terminal-phase Alzheimer's subjects, which were similar in morphology and size to the degenerating noradrenergic fiber clusters found in *Sstr2*$^{-/-}$ mice. However, in addition to noradrenergic fibers, TH also labels a substantial number of

dopaminergic fibers in the human neocortex [43]. More advanced fixation techniques [43], allowing the application of the DBH or NET antibodies to human brain, are required for the detailed morphological and quantitative spatial analysis of noradrenergic axonal arborization in human post mortem brain samples from neurodegenerative diseases.

The behavioral phenotype of *Sstr2*$^{-/-}$ mice

Sstr2 knockout/LacZ knockin mice show impaired motor coordination [6], and another *Sstr2* knockout strain exhibits locomotor and exploratory deficits, as well as enhanced anxiety-like behavior (*SI-D3*). Moreover, enhanced glutamate transmission in the hippocampus of young *Sstr2* knockouts was described [31,113], perhaps due to reduced SST-mediated inhibition of glutamate release [33].

This *Sstr2*$^{-/-}$ behavioral phenotype is comparable with a dysfunctional noradrenergic system. Thus, *DBH*$^{-/-}$ mice show deficits in social discrimination, reduced exploratory activity in novel environments, decreased locomotor activity in novel stimulation and impaired motor-coordination [66,86]. Moreover, rats with axonal NA degeneration after treatment with the neurotoxin DSP4 exhibit neophobic behavior [50], very much resembling the *Sstr2*$^{-/-}$ behavioral phenotype.

Implications for neurological and mental disorders

SST was found to be the most consistently reduced neuropeptide in Alzheimer's disease [20,27,89,58,19]. The SST deficit correlates well with the dementia score in Alzheimer's disease but less so with progression of neuropathology [30], indicating association mainly with cognitive impairment [112,34].

Pre-clinical and clinical trials have indicated that a SST release-enhancer (FK962) or the SST analogue octreotide (sandostatin) improves memory [24,102], but finally none of

them passed the phase 3 trial. Recent pre-clinical studies, however, reported that FK962 combined with the AChE inhibitor donepesil (Aricept) has a significantly greater effect on cognition than either compound alone [69]. This supports the notion on the necessity of combined therapy of Alzheimer's disease, a multisystem disorder affecting multiple neuronal population [29].

Several clinical and experimental studies indicate that the SST system is also implicated in stress, anxiety and depression [64], and there is now direct evidence that, in fact, the receptor involved is SSTR2 [32,33,118]. Notably, depression is a leading neuropsychiatric complication in Alzheimer's disease [94], and an association with chronic life stress and later-life cognitive dysfunction has been proposed [46].

Concluding remarks

The main goal of our studies was to elucidate potential factors underlying the well documented vulnerability of the noradrenergic LC neurons in Alzheimer's disease. It has been proposed that the evolutionary fast and large increase in brain volume, including the expansion of the long and poorly myelinated diffuse cortical projections of subcortical nuclei, such as LC, have made these evolutionary old, subcortical structures more vulnerable to age-related challenges specifically in the human brain [14,15]. Consequently, the currently used Alzheimer mouse models do not appear suitable for the study of pathomechanisms responsible for neurodegeneration of the LC in Alzheimer's disease. Therefore, we turned to another experimental approach based on the facts that (i) SST is significantly decreased in the cortex and hypothalamus in Alzheimer's disease, and (ii) one of its receptors, the SSTR2, is highly expressed not only in rodent but also, as shown here, in the human LC.

The present findings of an early, selective and global axonal degeneration of noradrenergic projections in *Sstr2*$^{-/-}$ mice suggest that SSTR2 is critically involved in the maintenance and integrity of noradrenergic system, a widespread brain network of

fundamental importance for the regulation of arousal, stress and emotions, memory functions and motor coordination. Based on these animal data, we propose that an early decrease of *SSTR2* expression in the LC of Alzheimer's disease subjects, in agreement with the present results on Alzheimer brains, may be an important component of the vulnerability of LC projections. Our data supports a scenario in which reduced SST neurotransmission and SSTR2 receptor mediated signaling in noradrenergic LC neurons contributes to the loss of noradrenergic innervation of the forebrain in Alzheimer's disease. Noradrenergic impairment results in mood and other behavioral changes and accelerates AD pathology as shown by others [98,52,48,85]. Finally, our results point to the SSTR2 as potential drug target for neurodegenerative and/or neuropsychiatric disorders, perhaps as part of a combined pharmacotherapy.

Acknowledgements We are grateful for the excellent technical assistance of Blanca Silva-Lopez, Agnieszka Limiszweska and Anita Bergstrand. We thank Professor Tamas Freund, Laboratory of Cerebral Cortex Research, Institute of Experimental Medicine of the Hungarian Academy of Sciences, Budapest, Hungary for generous donation of human brain tissue. Thanks to Professors Staffan Cullheim, Department of Neuroscience, Karolinska Institutet, Stockholm and Bengt Winblad, Department of Neurobiology, Care Sciences and Society, Alzheimer Disease Research Center, Center for Alzheimer Research, Division for Neurogeriatrics, Karolinska Institutet, Stockholm, for support, and to Dr. Zsolt Csaba (INSERM, Paris, France) and Dr. Szilvia Vas (Department of Pharmacodynamics, Semmelweis University, Budapest, Hungary) for valuable discussions. Thanks to Professor Charles Glabe, Dept. of Molecular Biology and Biochemistry, University of California at Irvine, Irvine, CA, for generous donation of the OC antibody.

This study was supported by the Swedish Research Council, Grants from Karolinska Institutet, the Knut and Lars Hiertas Minne Foundation, the Novo Nordisk Foundation, the Petrus and Augusta Hedlunds Foundation, the Alzheimerfonden (grant 03-216) and the Hungarian National Brain Research Program (KTIA-NEP-13-1-2013-001). The Authors do not report any conflict of interest.

Conflict of Interest The Authors do not report any conflict of interest.

.

Ethical approval All procedures performed in studies involving human participants were in accordance with the ethical standards of the institutional and/or national research committee and with the 1964 Helsinki declaration and its later amendments or comparable ethical standards.

References

1. Adams JC (1992) Biotin amplification of biotin and horseradish peroxidase signals in histochemical stains. J Histochem Cytochem 40:1457-1463
2. Adolfsson R, Gottfries CG, Roos BE, Winblad B (1979) Changes in the brain catecholamines in patients with dementia of Alzheimer type. The British journal of psychiatry : the journal of mental science 135:216-223
3. Adori C, Ando RD, Szekeres M, Gutknecht L, Kovacs GG, Hunyady L, Lesch KP, Bagdy G (2011) Recovery and aging of serotonergic fibers after single and intermittent MDMA treatment in Dark Agouti rat. The Journal of comparative neurology 519:2353-2378. doi:10.1002/cne.22631
4. Adori C, Low P, Ando RD, Gutknecht L, Pap D, Truszka F, Takacs J, Kovacs GG, Lesch KP, Bagdy G (2011) Ultrastructural characterization of tryptophan hydroxylase 2-specific cortical serotonergic fibers and dorsal raphe neuronal cell bodies after MDMA treatment in rat. Psychopharmacology (Berl) 213:377-391. doi:10.1007/s00213-010-2041-2
5. Allen JP, Canty AJ, Schulz S, Humphrey PP, Emson PC, Young HM (2002) Identification of cells expressing somatostatin receptor 2 in the gastrointestinal tract of Sstr2 knockout/lacZ knockin mice. The Journal of comparative neurology 454:329-340. doi:10.1002/cne.10466
6. Allen JP, Hathway GJ, Clarke NJ, Jowett MI, Topps S, Kendrick KM, Humphrey PP, Wilkinson LS, Emson PC (2003) Somatostatin receptor 2 knockout/lacZ knockin mice show impaired motor coordination and reveal sites of somatostatin action within the striatum. Eur J Neurosci 17:1881-1895
7. Armstrong DM, Hersh LB, Gage FH (1988) Morphologic alterations of cholinergic processes in the neocortex of aged rats. Neurobiology of aging 9:199-205
8. Aston-Jones G (2004) Locus coeruleus, A5 and A7 noradrenergic cell groups. In: Paxinos G (ed) The Rat Nervous System, vol 3rd ed. Elsevier, Amsterdam, pp 259-264
9. Aston-Jones G, Rajkowski J, Kubiak P, Valentino RJ, Shipley MT (1996) Role of the locus coeruleus in emotional activation. Prog Brain Res 107:379-402
10. Attems J, Thal DR, Jellinger KA (2012) The relationship between subcortical tau pathology and Alzheimer's disease. Biochem Soc Trans 40:711-715. doi:10.1042/BST20120034
11. Berridge CW, Waterhouse BD (2003) The locus coeruleus-noradrenergic system: modulation of behavioral state and state-dependent cognitive processes. Brain Res Brain Res Rev 42:33-84
12. Bondareff W, Mountjoy CQ, Roth M (1982) Loss of neurons of origin of the adrenergic projection to cerebral cortex (nucleus locus ceruleus) in senile dementia. Neurology 32:164-168
13. Braak H, Del Tredici K (2011) Alzheimer's pathogenesis: is there neuron-to-neuron propagation? Acta neuropathologica 121:589-595. doi:10.1007/s00401-011-0825-z
14. Braak H, Del Tredici K (2011) The pathological process underlying Alzheimer's disease in individuals under thirty. Acta neuropathologica 121:171-181. doi:10.1007/s00401-010-0789-4
15. Braak H, Del Tredici K (2012) Where, when, and in what form does sporadic Alzheimer's disease begin? Curr Opin Neurol 25:708-714. doi:10.1097/WCO.0b013e32835a3432
16. Brazeau P, Vale W, Burgus R, Ling N, Butcher M, Rivier J, Guillemin R (1973) Hypothalamic polypeptide that inhibits the secretion of immunoreactive pituitary growth hormone. Science 179:77-79
17. Bremner JD, Krystal JH, Southwick SM, Charney DS (1996) Noradrenergic mechanisms in stress and anxiety: I. Preclinical studies. Synapse 23:28-38. doi:10.1002/(SICI)1098-2396(199605)23:1<28::AID-SYN4>3.0.CO;2-J [pii]

10.1002/(SICI)1098-2396(199605)23:1<28::AID-SYN4>3.0.CO;2-J
18. Bremner JD, Krystal JH, Southwick SM, Charney DS (1996) Noradrenergic mechanisms in stress and anxiety: II. Clinical studies. Synapse 23:39-51. doi:10.1002/(SICI)1098-2396(199605)23:1<39::AID-SYN5>3.0.CO;2-I [pii]

10.1002/(SICI)1098-2396(199605)23:1<39::AID-SYN5>3.0.CO;2-I
19. Burbach JP (2010) Neuropeptides from concept to online database www.neuropeptides.nl. Eur J Pharmacol 626:27-48. doi:S0014-2999(09)00904-2 [pii]

10.1016/j.ejphar.2009.10.015
20. Burgos-Ramos E, Hervas-Aguilar A, Aguado-Llera D, Puebla-Jimenez L, Hernandez-Pinto AM, Barrios V, Arilla-Ferreiro E (2008) Somatostatin and Alzheimer's disease. Mol Cell Endocrinol 286:104-111. doi:10.1016/j.mce.2008.01.014
21. Carpentier V, Vaudry H, Laquerriere A, Tayot J, Leroux P (1996) Distribution of somatostatin receptors in the adult human brainstem. Brain research 734:135-148
22. Chan-Palay V, Asan E (1989) Alterations in catecholamine neurons of the locus coeruleus in senile dementia of the Alzheimer type and in Parkinson's disease with and without dementia and depression. The Journal of comparative neurology 287:373-392. doi:10.1002/cne.902870308
23. Chessell IP, Black MD, Feniuk W, Humphrey PP (1996) Operational characteristics of somatostatin receptors mediating inhibitory actions on rat locus coeruleus neurones. Br J Pharmacol 117:1673-1678
24. Craft S, Asthana S, Newcomer JW, Wilkinson CW, Matos IT, Baker LD, Cherrier M, Lofgreen C, Latendresse S, Petrova A, Plymate S, Raskind M, Grimwood K, Veith RC (1999) Enhancement of memory in Alzheimer disease with insulin and somatostatin, but not glucose. Arch Gen Psychiatry 56:1135-1140
25. Cross AJ, Crow TJ, Perry EK, Perry RH, Blessed G, Tomlinson BE (1981) Reduced dopamine-beta-hydroxylase activity in Alzheimer's disease. British medical journal 282:93-94
26. Dahlström A, Fuxe K (1964) Evidence for the existence of monoamine neurons in the central nervous system. I. Demonstration of monoamines in the cell bodies of brainstem neurons. Acta Physiol Scand 62:1-55
27. Davies P, Katzman R, Terry RD (1980) Reduced somatostatin-like immunoreactivity in cerebral cortex from cases of Alzheimer disease and Alzheimer senile dementa. Nature 288:279-280
28. De Martino C, Zamboni L (1967) Silver methenamine stain for electron microscopy. J Ultrastruct Res 19:273-282
29. Doraiswamy PM, Xiong GL (2006) Pharmacological strategies for the prevention of Alzheimer's disease. Expert Opin Pharmacother 7:1-10. doi:10.1517/14656566.7.1.S1
30. Dournaud P, Delaere P, Hauw JJ, Epelbaum J (1995) Differential correlation between neurochemical deficits, neuropathology, and cognitive status in Alzheimer's disease. Neurobiology of aging 16:817-823
31. Dutar P, Vaillend C, Viollet C, Billard JM, Potier B, Carlo AS, Ungerer A, Epelbaum J (2002) Spatial learning and synaptic hippocampal plasticity in type 2 somatostatin receptor knock-out mice. Neuroscience 112:455-466
32. Engin E, Stellbrink J, Treit D, Dickson CT (2008) Anxiolytic and antidepressant effects of intracerebroventricularly administered somatostatin: behavioral and neurophysiological evidence. Neuroscience 157:666-676. doi:10.1016/j.neuroscience.2008.09.037
33. Engin E, Treit D (2009) Anxiolytic and antidepressant actions of somatostatin: the role of sst2 and sst3 receptors. Psychopharmacology (Berl) 206:281-289. doi:10.1007/s00213-009-1605-5
34. Epelbaum J (1986) Somatostatin in the central nervous system: physiology and pathological modifications. Prog Neurobiol 27:63-100. doi:0301-0082(86)90012-2 [pii]
35. Epelbaum J, Bluet-Pajot MT, Llorens-Cortes C, Kordon C, Mounier F, Senut MC, Videau C (1990) 125I-[Tyr0,D-Trp8]somatostatin-14 binding sites in the locus coeruleus of the rat are located on both ascending and descending projecting noradrenergic cells. Peptides 11:21-27
36. Epelbaum J, Guillou JL, Gastambide F, Hoyer D, Duron E, Viollet C (2009) Somatostatin, Alzheimer's disease and cognition: an old story coming of age? Prog Neurobiol 89:153-161. doi:10.1016/j.pneurobio.2009.07.002

37. Farris TW, Butcher LL, Oh JD, Woolf NJ (1995) Trophic-factor modulation of cortical acetylcholinesterase reappearance following transection of the medial cholinergic pathway in the adult rat. Exp Neurol 131:180-192
38. Ferriero DM, Sheldon RA, Messing RO (1994) Somatostatin enhances nerve growth factor-induced neurite outgrowth in PC12 cells. Brain Res Dev Brain Res 80:13-18
39. Foote SL, Bloom FE, Aston-Jones G (1983) Nucleus locus ceruleus: new evidence of anatomical and physiological specificity. Physiol Rev 63:844-914
40. Fuxe K, Hökfelt T, Ungerstedt U (1970) Central monoaminergic tracts. In: Clark WG, Del Guidice J (eds) Principles of Psychopharmacology. pp 87-96
41. Gagne C, Moyse E, Kocher L, Bour H, Pujol JF (1990) Light-microscopic localization of somatostatin binding sites in the locus coeruleus of the rat. Brain research 530:196-204
42. Gahete MD, Rubio A, Duran-Prado M, Avila J, Luque RM, Castano JP (2010) Expression of Somatostatin, cortistatin, and their receptors, as well as dopamine receptors, but not of neprilysin, are reduced in the temporal lobe of Alzheimer's disease patients. J Alzheimers Dis 20:465-475. doi:10.3233/JAD-2010-1385
43. Gaspar P, Berger B, Febvret A, Vigny A, Henry JP (1989) Catecholamine innervation of the human cerebral cortex as revealed by comparative immunohistochemistry of tyrosine hydroxylase and dopamine-beta-hydroxylase. The Journal of comparative neurology 279:249-271. doi:10.1002/cne.902790208
44. German DC, Manaye KF, White CL, 3rd, Woodward DJ, McIntire DD, Smith WK, Kalaria RN, Mann DM (1992) Disease-specific patterns of locus coeruleus cell loss. Ann Neurol 32:667-676. doi:10.1002/ana.410320510
45. German DC, Nelson O, Liang F, Liang CL, Games D (2005) The PDAPP mouse model of Alzheimer's disease: locus coeruleus neuronal shrinkage. The Journal of comparative neurology 492:469-476. doi:10.1002/cne.20744
46. Greenberg MS, Tanev K, Marin MF, Pitman RK (2014) Stress, PTSD, and dementia. Alzheimers Dement 10:S155-165. doi:10.1016/j.jalz.2014.04.008
47. Grzanna R, Fritschy JM (1991) Efferent projections of different subpopulations of central noradrenaline neurons. Prog Brain Res 88:89-101
48. Haglund M, Sjobeck M, Englund E (2006) Locus ceruleus degeneration is ubiquitous in Alzheimer's disease: possible implications for diagnosis and treatment. Neuropathology 26:528-532
49. Hammerschmidt T, Kummer MP, Terwel D, Martinez A, Gorji A, Pape HC, Rommelfanger KS, Schroeder JP, Stoll M, Schultze J, Weinshenker D, Heneka MT (2013) Selective loss of noradrenaline exacerbates early cognitive dysfunction and synaptic deficits in APP/PS1 mice. Biol Psychiatry 73:454-463. doi:10.1016/j.biopsych.2012.06.013
50. Harro J, Oreland L, Vasar E, Bradwejn J (1995) Impaired exploratory behaviour after DSP-4 treatment in rats: implications for the increased anxiety after noradrenergic denervation. Eur Neuropsychopharmacol 5:447-455
51. Helyes Z, Pinter E, Sandor K, Elekes K, Banvolgyi A, Keszthelyi D, Szoke E, Toth DM, Sandor Z, Kereskai L, Pozsgai G, Allen JP, Emson PC, Markovics A, Szolcsanyi J (2009) Impaired defense mechanism against inflammation, hyperalgesia, and airway hyperreactivity in somatostatin 4 receptor gene-deleted mice. Proc Natl Acad Sci U S A 106:13088-13093. doi:10.1073/pnas.0900681106
52. Heneka MT, Nadrigny F, Regen T, Martinez-Hernandez A, Dumitrescu-Ozimek L, Terwel D, Jardanhazi-Kurutz D, Walter J, Kirchhoff F, Hanisch UK, Kummer MP (2010) Locus ceruleus controls Alzheimer's disease pathology by modulating microglial functions through norepinephrine. Proc Natl Acad Sci U S A 107:6058-6063. doi:10.1073/pnas.0909586107
53. Horgan J, Miguel-Hidalgo JJ, Thrasher M, Bissette G (2007) Longitudinal brain corticotropin releasing factor and somatostatin in a transgenic mouse (TG2576) model of Alzheimer's disease. J Alzheimers Dis 12:115-127

54. Hoyer D, Bell GI, Berelowitz M, Epelbaum J, Feniuk W, Humphrey PP, O'Carroll AM, Patel YC, Schonbrunn A, Taylor JE, et al. (1995) Classification and nomenclature of somatostatin receptors. Trends Pharmacol Sci 16:86-88. doi:S0165-6147(00)88988-9 [pii]
55. Inoue M, Nakajima S, Nakajima Y (1988) Somatostatin induces an inward rectification in rat locus coeruleus neurones through a pertussis toxin-sensitive mechanism. J Physiol 407:177-198
56. Kampf C, Olsson I, Ryberg U, Sjostedt E, Ponten F (2012) Production of tissue microarrays, immunohistochemistry staining and digitalization within the human protein atlas. Journal of visualized experiments : JoVE. doi:10.3791/3620
57. Kehr J YT (2006) Monitoring brain chemical signals by microdialysis, vol 6. In: Encyclopedia of Sensors. American Scientific Publishers, USA,
58. Kowall NW, Beal MF (1988) Cortical somatostatin, neuropeptide Y, and NADPH diaphorase neurons: normal anatomy and alterations in Alzheimer's disease. Ann Neurol 23:105-114. doi:10.1002/ana.410230202
59. Krantic S, Robitaille Y, Quirion R (1992) Deficits in the somatostatin SS1 receptor sub-type in frontal and temporal cortices in Alzheimer's disease. Brain research 573:299-304
60. Kummer MP, Hammerschmidt T, Martinez A, Terwel D, Eichele G, Witten A, Figura S, Stoll M, Schwartz S, Pape HC, Schultze JL, Weinshenker D, Heneka MT (2014) Ear2 deletion causes early memory and learning deficits in APP/PS1 mice. The Journal of neuroscience : the official journal of the Society for Neuroscience 34:8845-8854. doi:10.1523/JNEUROSCI.4027-13.2014
61. Laboratory J http://jaxmice.jax.org/strain/005844.html.
62. Le Maitre E, Barde SS, Palkovits M, Diaz-Heijtz R, Hokfelt TG (2013) Distinct features of neurotransmitter systems in the human brain with focus on the galanin system in locus coeruleus and dorsal raphe. Proc Natl Acad Sci U S A 110:E536-545. doi:10.1073/pnas.1221378110
63. Levi-Montalcini R (1987) The nerve growth factor 35 years later. Science 237:1154-1162
64. Lin LC, Sibille E (2013) Reduced brain somatostatin in mood disorders: a common pathophysiological substrate and drug target? Front Pharmacol 4:110. doi:10.3389/fphar.2013.00110
65. Mann DM, Lincoln J, Yates PO, Stamp JE, Toper S (1980) Changes in the monoamine containing neurones of the human CNS in senile dementia. Br J Psychiatry 136:533-541
66. Marino MD, Bourdelat-Parks BN, Cameron Liles L, Weinshenker D (2005) Genetic reduction of noradrenergic function alters social memory and reduces aggression in mice. Behav Brain Res 161:197-203. doi:10.1016/j.bbr.2005.02.005
67. Masaya Tohyama KT (1998) Atlas of Neuroactive Substances and Their Receptors in the Rat. Oxford University Press, New York
68. Masuko S, Nakajima Y, Nakajima S, Yamaguchi K (1986) Noradrenergic neurons from the locus ceruleus in dissociated cell culture: culture methods, morphology, and electrophysiology. The Journal of neuroscience : the official journal of the Society for Neuroscience 6:3229-3241
69. McCarthy AD, Owens IJ, Bansal AT, McTighe SM, Bussey TJ, Saksida LM (2011) FK962 and donepezil act synergistically to improve cognition in rats: potential as an add-on therapy for Alzheimer's disease. Pharmacol Biochem Behav 98:76-80. doi:10.1016/j.pbb.2010.11.019
70. McMillan PJ, White SS, Franklin A, Greenup JL, Leverenz JB, Raskind MA, Szot P (2011) Differential response of the central noradrenergic nervous system to the loss of locus coeruleus neurons in Parkinson's disease and Alzheimer's disease. Brain research 1373:240-252. doi:10.1016/j.brainres.2010.12.015
71. Melander T, Hökfelt T, Rokaeus A, Cuello AC, Oertel WH, Verhofstad A, Goldstein M (1986) Coexistence of galanin-like immunoreactivity with catecholamines, 5-hydroxytryptamine, GABA and neuropeptides in the rat CNS. The Journal of neuroscience : the official journal of the Society for Neuroscience 6:3640-3654
72. Moore RY, Bloom FE (1979) Central catecholamine neuron systems: anatomy and physiology of the norepinephrine and epinephrine systems. Annu Rev Neurosci 2:113-168. doi:10.1146/annurev.ne.02.030179.000553

73. Morilak DA, Barrera G, Echevarria DJ, Garcia AS, Hernandez A, Ma S, Petre CO (2005) Role of brain norepinephrine in the behavioral response to stress. Prog Neuropsychopharmacol Biol Psychiatry 29:1214-1224. doi:S0278-5846(05)00270-8 [pii]

10.1016/j.pnpbp.2005.08.007
74. Morrison JH, Rogers J, Scherr S, Benoit R, Bloom FE (1985) Somatostatin immunoreactivity in neuritic plaques of Alzheimer's patients. Nature 314:90-92
75. Murayama S, Saito Y (2004) Neuropathological diagnostic criteria for Alzheimer's disease. Neuropathology 24:254-260
76. Nemeroff CB, Kizer JS, Reynolds GP, Bissette G (1989) Neuropeptides in Alzheimer's disease: a postmortem study. Regul Pept 25:123-130
77. Nishimura A, Ueda S, Takeuchi Y, Matsushita H, Sawada T, Kawata M (1998) Vulnerability to aging in the rat serotonergic system. Acta neuropathologica 96:581-595
78. Norberg KA (1967) Transmitter histochemistry of the sympathetic adrenergic nervous system. Brain research 5:125-170
79. Olpe HR, Steinmann MW, Pozza MF, Haas HL (1987) Comparative investigations on the actions of ACTH1-24, somatostatin, neurotensin, substance P and vasopressin on locus coeruleus neuronal activity in vitro. Naunyn Schmiedebergs Arch Pharmacol 336:434-437
80. Palkovits M, Epelbaum J, Tapia-Arancibia L, Kordon C (1982) Somatostatin in catecholamine-rich nuclei of the brainstem. Neuropeptides 3:139-144
81. Palmer AM, Wilcock GK, Esiri MM, Francis PT, Bowen DM (1987) Monoaminergic innervation of the frontal and temporal lobes in Alzheimer's disease. Brain research 401:231-238
82. Paxinos G HX (1995) Atlas of the Human Brainstem. Academic Press Inc., San Diego
83. Peng I, Binder LI, Black MM (1986) Biochemical and immunological analyses of cytoskeletal domains of neurons. J Cell Biol 102:252-262
84. Ramos B, Baglietto-Vargas D, del Rio JC, Moreno-Gonzalez I, Santa-Maria C, Jimenez S, Caballero C, Lopez-Tellez JF, Khan ZU, Ruano D, Gutierrez A, Vitorica J (2006) Early neuropathology of somatostatin/NPY GABAergic cells in the hippocampus of a PS1xAPP transgenic model of Alzheimer's disease. Neurobiology of aging 27:1658-1672. doi:10.1016/j.neurobiolaging.2005.09.022
85. Robertson IH (2013) A noradrenergic theory of cognitive reserve: implications for Alzheimer's disease. Neurobiology of aging 34:298-308. doi:10.1016/j.neurobiolaging.2012.05.019
86. Rommelfanger KS, Edwards GL, Freeman KG, Liles LC, Miller GW, Weinshenker D (2007) Norepinephrine loss produces more profound motor deficits than MPTP treatment in mice. Proc Natl Acad Sci U S A 104:13804-13809. doi:10.1073/pnas.0702753104
87. Ronnback A, Sagelius H, Bergstedt KD, Naslund J, Westermark GT, Winblad B, Graff C (2012) Amyloid neuropathology in the single Arctic APP transgenic model affects interconnected brain regions. Neurobiology of aging 33:831 e811-839. doi:10.1016/j.neurobiolaging.2011.07.012
88. Ronnback A, Zhu S, Dillner K, Aoki M, Lilius L, Naslund J, Winblad B, Graff C (2011) Progressive neuropathology and cognitive decline in a single Arctic APP transgenic mouse model. Neurobiology of aging 32:280-292. doi:10.1016/j.neurobiolaging.2009.02.021
89. Rossor MN, Emson PC, Mountjoy CQ, Roth M, Iversen LL (1980) Reduced amounts of immunoreactive somatostatin in the temporal cortex in senile dementia of Alzheimer type. Neuroscience letters 20:373-377
90. Saito T, Iwata N, Tsubuki S, Takaki Y, Takano J, Huang SM, Suemoto T, Higuchi M, Saido TC (2005) Somatostatin regulates brain amyloid beta peptide Abeta42 through modulation of proteolytic degradation. Nat Med 11:434-439. doi:10.1038/nm1206
91. Savonenko A, Xu GM, Melnikova T, Morton JL, Gonzales V, Wong MP, Price DL, Tang F, Markowska AL, Borchelt DR (2005) Episodic-like memory deficits in the APPswe/PS1dE9 mouse model of Alzheimer's disease: relationships to beta-amyloid deposition and neurotransmitter abnormalities. Neurobiol Dis 18:602-617. doi:10.1016/j.nbd.2004.10.022

92. Schalling M, Seroogy K, Hökfelt T, Chai SY, Hallman H, Persson H, Larhammar D, Ericsson A, Terenius L, Graffi J, et al. (1988) Neuropeptide tyrosine in the rat adrenal gland--immunohistochemical and in situ hybridization studies. Neuroscience 24:337-349
93. Schatzberg F, Schildkraut JJ (1995) Recent studies on norepinephrine systems in mood disorders. In: Bloom FE, Kupfer DJ (eds) Psychopharmacology. Raven Press, New York, pp 911-920
94. Sepehry AA, Lee PE, Hsiung GY, Beattie BL, Jacova C (2012) Effect of selective serotonin reuptake inhibitors in Alzheimer's disease with comorbid depression: a meta-analysis of depression and cognitive outcomes. Drugs Aging 29:793-806. doi:10.1007/s40266-012-0012-5
95. Shi TJ, Xiang Q, Zhang MD, Barde S, Kai-Larsen Y, Fried K, Josephson A, Gluck L, Deyev SM, Zvyagin AV, Schulz S, Hokfelt T (2014) Somatostatin and its 2A receptor in dorsal root ganglia and dorsal horn of mouse and human: expression, trafficking and possible role in pain. Mol Pain 10:12. doi:1744-8069-10-12 [pii]

10.1186/1744-8069-10-12
96. Stengel A, Rivier J, Tache Y (2013) Modulation of the adaptive response to stress by brain activation of selective somatostatin receptor subtypes. Peptides 42:70-77. doi:10.1016/j.peptides.2012.12.022
97. Szabadi E (2013) Functional neuroanatomy of the central noradrenergic system. Journal of psychopharmacology 27:659-693. doi:10.1177/0269881113490326
98. Szot P (2012) Common factors among Alzheimer's disease, Parkinson's disease, and epilepsy: possible role of the noradrenergic nervous system. Epilepsia 53 Suppl 1:61-66. doi:10.1111/j.1528-1167.2012.03476.x
99. Szot P, White SS, Greenup JL, Leverenz JB, Peskind ER, Raskind MA (2006) Compensatory changes in the noradrenergic nervous system in the locus ceruleus and hippocampus of postmortem subjects with Alzheimer's disease and dementia with Lewy bodies. The Journal of neuroscience : the official journal of the Society for Neuroscience 26:467-478. doi:10.1523/JNEUROSCI.4265-05.2006
100. Tatemoto K, Rokaeus A, Jornvall H, McDonald TJ, Mutt V (1983) Galanin - a novel biologically active peptide from porcine intestine. FEBS Lett 164:124-128. doi:0014-5793(83)80033-7 [pii]
101. Thoss VS, Perez J, Duc D, Hoyer D (1995) Embryonic and postnatal mRNA distribution of five somatostatin receptor subtypes in the rat brain. Neuropharmacology 34:1673-1688
102. Tokita K, Inoue T, Yamazaki S, Wang F, Yamaji T, Matsuoka N, Mutoh S (2005) FK962, a novel enhancer of somatostatin release, exerts cognitive-enhancing actions in rats. Eur J Pharmacol 527:111-120. doi:10.1016/j.ejphar.2005.10.022
103. Tomlinson BE, Irving D, Blessed G (1981) Cell loss in the locus coeruleus in senile dementia of Alzheimer type. J Neurol Sci 49:419-428
104. Toppila J, Niittymaki P, Porkka-Heiskanen T, Stenberg D (2000) Intracerebroventricular and locus coeruleus microinjections of somatostatin antagonist decrease REM sleep in rats. Pharmacol Biochem Behav 66:721-727
105. Toth K, Eross L, Vajda J, Halasz P, Freund TF, Magloczky Z (2010) Loss and reorganization of calretinin-containing interneurons in the epileptic human hippocampus. Brain : a journal of neurology 133:2763-2777. doi:10.1093/brain/awq149
106. Ueda S, Aikawa M, Ishizuya-Oka A, Yamaoka S, Koibuchi N, Yoshimoto K (2000) Age-related dopamine deficiency in the mesostriatal dopamine system of zitter mutant rats: regional fiber vulnerability in the striatum and the olfactory tubercle. Neuroscience 95:389-398
107. Vale W, Brazeau P, Rivier C, Brown M, Boss B, Rivier J, Burgus R, Ling N, Guillemin R (1975) Somatostatin. Recent Prog Horm Res 31:365-397
108. van de Nes JA, Konermann S, Nafe R, Swaab DF (2006) Beta-protein/A4 deposits are not associated with hyperphosphorylated tau in somatostatin neurons in the hypothalamus of Alzheimer's disease patients. Acta neuropathologica 111:126-138. doi:10.1007/s00401-005-0018-8

109. van Luijtelaar MG, Steinbusch HW, Tonnaer JA (1988) Aberrant morphology of serotonergic fibers in the forebrain of the aged rat. Neuroscience letters 95:93-96
110. van Luijtelaar MG, Tonnaer JA, Steinbusch HW (1992) Aging of the serotonergic system in the rat forebrain: an immunocytochemical and neurochemical study. Neurobiology of aging 13:201-215
111. Vepsalainen S, Helisalmi S, Koivisto AM, Tapaninen T, Hiltunen M, Soininen H (2007) Somatostatin genetic variants modify the risk for Alzheimer's disease among Finnish patients. J Neurol 254:1504-1508. doi:10.1007/s00415-007-0539-2
112. Viollet C, Lepousez G, Loudes C, Videau C, Simon A, Epelbaum J (2008) Somatostatinergic systems in brain: networks and functions. Mol Cell Endocrinol 286:75-87. doi:10.1016/j.mce.2007.09.007
113. Viollet C, Vaillend C, Videau C, Bluet-Pajot MT, Ungerer A, L'Heritier A, Kopp C, Potier B, Billard J, Schaeffer J, Smith RG, Rohrer SP, Wilkinson H, Zheng H, Epelbaum J (2000) Involvement of sst2 somatostatin receptor in locomotor, exploratory activity and emotional reactivity in mice. Eur J Neurosci 12:3761-3770
114. Watabe Y, Yoshimoto K, Eguchi M, Ueda S (2005) Degeneration of monoaminergic fibers in the aged micrencephalic rat. Neuroscience letters 385:82-86. doi:10.1016/j.neulet.2005.05.020
115. Weinshenker D (2008) Functional consequences of locus coeruleus degeneration in Alzheimer's disease. Curr Alzheimer Res 5:342-345
116. Xu ZQ, Shi TJ, Hökfelt T (1998) Galanin/GMAP- and NPY-like immunoreactivities in locus coeruleus and noradrenergic nerve terminals in the hippocampal formation and cortex with notes on the galanin-R1 and -R2 receptors. The Journal of comparative neurology 392:227-251
117. Xue S, Jia L, Jia J (2009) Association between somatostatin gene polymorphisms and sporadic Alzheimer's disease in Chinese population. Neuroscience letters 465:181-183. doi:10.1016/j.neulet.2009.09.002
118. Yeung M, Treit D (2012) The anxiolytic effects of somatostatin following intra-septal and intra-amygdalar microinfusions are reversed by the selective sst2 antagonist PRL2903. Pharmacol Biochem Behav 101:88-92. doi:10.1016/j.pbb.2011.12.012
119. Zarow C, Lyness SA, Mortimer JA, Chui HC (2003) Neuronal loss is greater in the locus coeruleus than nucleus basalis and substantia nigra in Alzheimer and Parkinson diseases. Arch Neurol 60:337-341

Figure legends

Fig. 1 Somatodendritic SSTR2a immunolocalization in human LC. (**a**) Low-power overview of human LC (TH+SSTR2a double labeling). (**b**) Schematic representation of the dorsolateral part of human brainstem at the level of Obex +23, adopted from the human brainstem atlas of Paxinos and Huang [82]. The box in B shows area depicted in A. (**c**) Higher magnification of the boxed zone ***c*** in panel A. Note the somatodendritic localization of SSTR2a in several TH-IR NA LC neurons (arrowheads). (**d**) High magnification of the boxed zone ***d*** in panel A. 0.5-μm-thick optical layer micrograph of an individual neuron, confocal microscopy. 4V: fourth ventricle; me5: mesenchephalic trigeminal tract. Scale bars: 400 μm in a; 100 μm in c; 10 μm in d.

Fig. 2 Decreased SSTR2 expression in the LC in Alzheimer's disease (AD). (**a**) Average Ct values of control cases for all examined genes. *SSTR2* is expressed at levels almost as high as for TH, compared to *GAL* and *GALR3*, the most abundant galanin receptor in LC [62]. Note that the Ct values are inversely proportional with the amount of detected RNA. (**b**) The expression level of *SSTR2* is significantly decreased in Alzheimer's disease Braak III-IV and V-VI stages. *MAP2* expression is decreased only in the Braak III-IV stage. Relative expression levels (fold changes) were calculated by normalizing Ct values to *TUBB3* as a reference gene and subsequently to the average of controls. Fold-changes were calculated by the comparative Ct method ($2^{-\Delta\Delta CT}$). Values for controls were set to 1.00. (**c**) Relative expression level of *SSTR2,* where Ct values were normalized to *TUBB3*, *ACTIN* or *GAPDH* as reference genes. Statistical analysis: one-way ANOVA and Fisher Test for *post-hoc* test for comparisons (N=8, N=5, N=7, control, AD Braak III-IV, AD Braak V-VI, respectively; *significant difference between control and AD cases, $^{\#}$significant difference between AD Braak III-IV and AD Braak V-VI cases). Data are expressed as mean ± SEM.

Fig. 3 Aberrant TH-immunoreactive fibers in the temporal cortex of Alzheimer's disease brains (**a**) Tissue micro-array (TMA) slide with 1-mm-diameter temporal cortical punch samples of 7 Alzheimer's disease subjects (in squared boxes) and 9 control subjects. (The TMA slide also contained 10 DLB cases, which were not analyzed in the present study). The slides were triple-stained for TH, amyloid-β and Tau-PHF and were counterstained with the nuclear staining DAPI. Whole slide immunofluorescence for Tau-PHF (AT8) is demonstrated. (**b**–**c**) Examples of morphologically intact TH-IR fibers from an age-matched control case (arrowheads). The boxed zone in b is enlarged in c. Note that there is no any amyloid-β or tau PHF immunostaining in the control tissue. (***d–g***) Examples of aberrant, cluster-like TH-IR structures containing swollen varicosities from two Alzheimer's frontal cortex samples (AD brain 1 and 2) are shown. Dystrophic neurites are immunostained for tau-PHF throughout the samples (d, f) and amyloid plaques are stained for amyloid-β (d, stars). The boxed fiber clusters in d and f (triple staining) are enlarged in e and g, respectively (TH staining only). Scale bars: 2,000 μm in a; 50 μm in b, d and f; 25 μm in e and g, 20 μm in c.

Fig. 4 Immunohistochemical staining of Alzheimer and control brains in temporal cortex samples. (**a–d**) Representative micrographs from a tissue micro-array slide triple-stained for SST, amyloid-β and Tau-PHF and counterstained with Dapi. In the control sample, a dense network of SST-IR processes was strongly immunostained (a-b). In the Alzheimer samples, SST-like immunoreactivity significantly decreased: only sparse fibers were noted throughout the samples (c-d). In contrast, amyloid-β IR depositions and tau-PHF IR dystrophic neurits and neurofibrillary tangles (* in d) were frequently noted in the AD samples but not in the control samples (c-d vs. a-b). Arrows in d indicate tau-PHF^{+} dystrophic neurites/terminals around the amyloid-β^{+} senile plaques. Boxed zones in a and c are enlarged in b and d, respectively. Scale bars: 100 μm in c applies for a and c; 50 μm in d, applies for b and d. **(e–**

g) Quantitative evaluation of SST, amyloid-β and tau-PHF immunoreactivity in the TMA slide (densitometry analysis). Note that the immunoreactivity for amyloid-β (e) and tau-PHF (f) significantly increases, while the SST-like immunoreactivity significantly decreases (g) in the Alzheimer's samples. Statistical analysis: Student's t-test for independent samples (N = 7 and 9, Alzheimer's disease and control samples, respectively).

Fig. 5 SSTR2a protein expressions in mouse NA cell groups. (**a**–**b**) Noradrenergic neurons in the LC (a, low power overview; a*, high power micrographs) and all other examined NA cell groups (A1, A2, A6r, A7, panel b) exhibit prominent somatodendritic SSTR2a localization. (**c**) Strong sstr2^{lacZ} staining in the LC neurons of *Sstr2*$^{-/-}$ mice (upper panels). No NET-IR (noradrenergic) neurons co-localize with Sstr1^{lacZ} or with Sstr4^{lacZ} staining in the LC of *Sstr1*$^{-/-}$ or *Sstr4*$^{-/-}$ animals, respectively (medial and lower panels, respectively). (**d**) TPH2-IR (serotonergic) neurons in the dorsal raphe, DAT-IR (dopaminergic) neurons in the substantia nigra pars compacta and VTA and ChAT-IR (cholinergic) neurons in the nucleus basalis Meynerti or in the nucleus of the horizontal limb of the diagonal band (HDB) do not show co-localization with SSTR2 in *WT* animals. Scale bars: 100 μm in a and c; 10 μm in a*; 50 μm in b and d.

Fig. 6 Selective noradrenergic axonal degeneration in Sstr2$^{-/-}$ animals. (**a**) *Sstr2*$^{-/-}$, but not Sstr1$^{-/-}$ or *Sstr4*$^{-/-}$ mice exhibit a substantially reduced density of TH-IR nerve terminals in the prefrontal cortex (FCtx). Aberrant large fiber clusters are also often detected (arrows). (**b**) The large TH-IR fibers clusters (arrows) are associated with activated microglial (Iba1-IR) or astroglial (GFAP-IR) cells. In contrast, astroglial or microglial cells exhibit normal morphology in *WT*s. (**c**) The noradrenergic marker DBH shows a reduced density of noradrenergic fibers, many of them with swollen profiles and cluster formations (left panel). Aberrant noradrenergic fibers and fiber clusters (arrows) are co-localized with the

neuropeptide galanin, known to be expressed in cortical and hippocampal noradrenergic fibers (and LC) [116]. (**d**) Serotonergic (TPH2-IR, FCtx), dopaminergic (DAT-IR, insular cortex) or cholinergic (ChAT-IR, FCtx) fibers do not show any signs of degeneration in *Sstr2*$^{-/-}$ mice, contrasting the noradrenergic fibers (NET, FCtx). (**e**) HPLC measurements of monoamine neurotransmitters (NA; DA; 5-HT) in 2-week- and 4-month-old *Sstr2*$^{-/-}$ and *WT* mice. NA levels were significantly decreased in the FCtx and hippocampus (Hippo) but not in the caudate-putamen (CPu) of 4-month-old *Sstr2*$^{-/-}$ mice. In the 2-week-old *Sstr2*$^{-/-}$ mice, there was a significant decrease in NA levels only in the Hippo and a slight but yet significant increase in the DA levels of CPu. Other monoamine levels were not significantly altered. Statistical analysis: three-way analysis of variance (ANOVA, variables: region, genotype, age) and Tukey Test for *post-hoc* comparisons (N = 5, $*P < 0.05$; $^{\#}P < 0.1$, trend to significance). Data are expressed as mean ± SEM. Scale bars: 100 μm in a, b and in c left panel; 50 μm c right panel; 200 μm in d.

Fig. 7 Detailed characterization of selective noradrenergic axonal degeneration. (**a**) The TH-IR fiber density is gradually decreased with age in the frontal cortex of *Sstr2*$^{-/-}$, compared to age-matched *WT*s. Statistical analysis: two-way analysis of variance (ANOVA, variables: genotype, age) and Tukey Test were used for *post-hoc* comparisons (N = 4, *P < 0.05). Data are expressed as mean ± SEM. (**b–c**) Single swollen varicosities/intervaricose connections and dense clustering of fibers with irregular fiber pattern (fiber clusters) were quantitatively determined in the fronto-parietal cortex of TH immunostained sections of *Sstr2*$^{-/-}$ mice. Statistical analysis: one-way ANOVA and Tukey Test for *post-hoc* comparisons (N = 4, *P < 0.05). Data are expressed as mean ± SEM. (**d–f, d*–f***) Overview of morphological alterations in the noradrenergic system of *Sstr2*$^{-/-}$ animals. The noradrenergic fiber density gradually decreases, while the number of aberrant fiber structures (swollen, enlarged varicosities, arrowheads in e*; fiber clusters, arrowheads in f–f*) gradually increases with

age. d, e, f: low power overviews of somatosensory-parietal-retrosplenial cortices; d*, e*, f*: higher magnification micrographs from somatosensory cortex. (**g–j)** Confocal analysis of aberrant noradrenergic structures (merged micrographs of 0.5-μm-thick optical layers along the Z-stack). The single swollen varicosities/intervaricose connections (5-7 μm in diameter; h, arrows) are easily identifiable due to their morphology and dense staining compared with neighboring normal noradrenergic fibers (g). The knot-like fiber clusters ('loose type', i; 'compact', j) comprise aggregated, irregular-shaped, tortuous fibers with a high number of concentrated swollen varicosities/intervaricose connections. These clusters are distinct and appear as an interruption of the adjacent normal fiber pattern. Their size varied approximately from 50 to 250 μm. The single swollen varicosities/intervaricose connections and the distinct fiber clusters are visualized in the same manner using antibodies to NET, TH or DBH. These aberrant structures are virtually not detected in the *WT*s. Scale bars: 500 μm in d, applies to d, e and f; 100 μm in f*, applies to d*, e* and f*; 25 μm in g, applied to g and h; 100 μm in i, applies to i and j.

Fig. 8 Distinct loss of noradrenergic fibers in the spinal cord. There is a marked decrease of the NET-IR fiber density in the lumbar spinal cord of a 4-month-old *Sstr2*$^{-/-}$ animal compared to *WT* (cf. b with a), but no large fiber clusters can be seen. The most pronounced fiber decrease is found in the dorsal horn (Rexed laminae I-IV). A moderate decrease is detected in Rexed laminae V-VIII. No apparent decrease in degeneration/fiber density is detected in Rexed X (around the central canal) or Rexed IX. CC: central canal. Scale bar: 200 μm in a applies to a and b.

Fig. 9 No signs of degeneration of LC cell bodies can be detected in Sstr2$^{-/-}$ mice up till 8 months-of-age. (**a**–**b**) TH immunostaining (FITC - green) and TO-PRO®-3 (far red, transformed digitally to red color) nuclear counterstaining of the LC from an 8-month-old *WT* (a) and a *Sstr2*$^{-/-}$ (b) mouse. (**c**–**d**) The number of TH-IR cell bodies and also their mean

somatic surface area do not show significant differences between the 8-month-old *Sstr2*$^{-/-}$ and their age-matched *WT* littermates. (**e**–**f**) TH in situ hybridization in 4-month-old *WT* (e) and *Sstr2*$^{-/-}$ (F) LC. (**g**–**h**) Summary of quantitative results from 4-month-old animals. TH, but not galanin expression is decreased in the *Sstr2*$^{-/-}$ compared to *WT* mice. Statistical analyses: Student's T-test for independent samples (N = 3, N = 5, c-d, g-h, respectively. $^{*}P < 0.05$). Data are expressed as mean ± SEM. Scale bar: 100 μm in a, applies to a, b, e and f.

Fig. 10 There is no noradrenergic degeneration in the peripheral nervous system. TH (a) neuropeptide Y (NPY, b) and SST2a (c) immunostaining of the superior cervical ganglion (SCG) of a *WT* animal is demonstrated. Note that the faint-moderate SST2a immunoreactivity in SCG is restricted only to a few neurons. NET immunostaining of jejunum (d-e) and salivary gland (f-g) of *Sstr2*$^{-/-}$ (e, g) and *WT* (d, f) littermates. No signs of axonal degeneration are found in the peripheral noradrenergic system. Scale bars: 200 μm in a, applies to all panels.

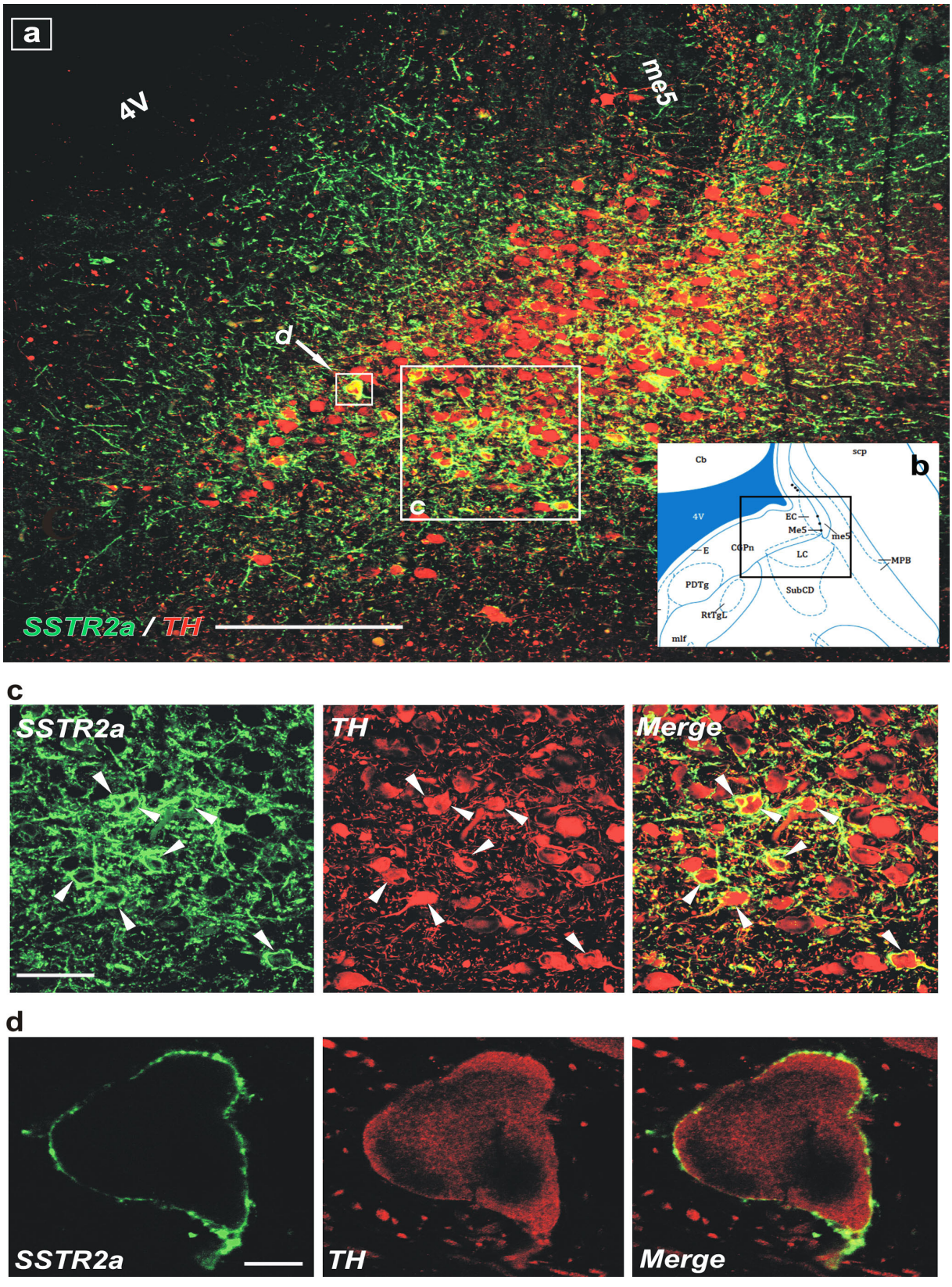
a
4V
me5
d
c
SSTR2a / TH
b
Cb
scp
4V
EC
Me5
me5
E
CGPn
LC
MPB
PDTg
SubCD
RtTgL
mlf
c
SSTR2a
TH
Merge
d
SSTR2a
TH
Merge

Figure 1

a

Gene	DBH	TH	GALR3	GAL	SSTR2	MAP2	TUBB3	ACTIN	GAPDH
Average Ct value of controls	23.84	25.13	34.31	28.64	26.71	21.82	22.64	21.36	20.27

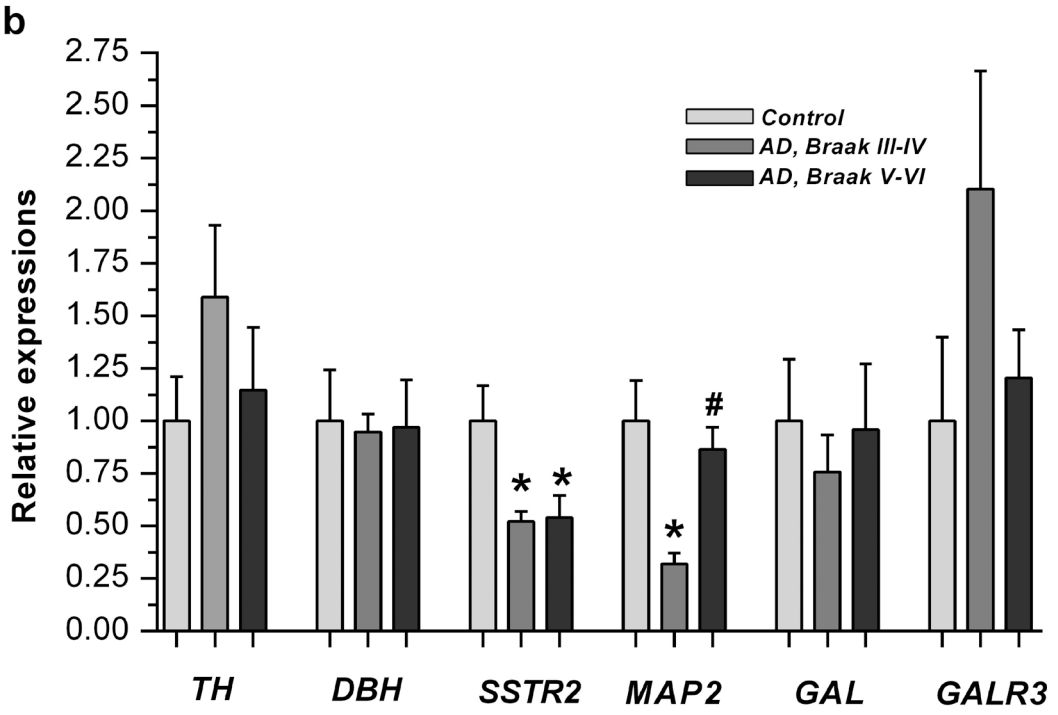

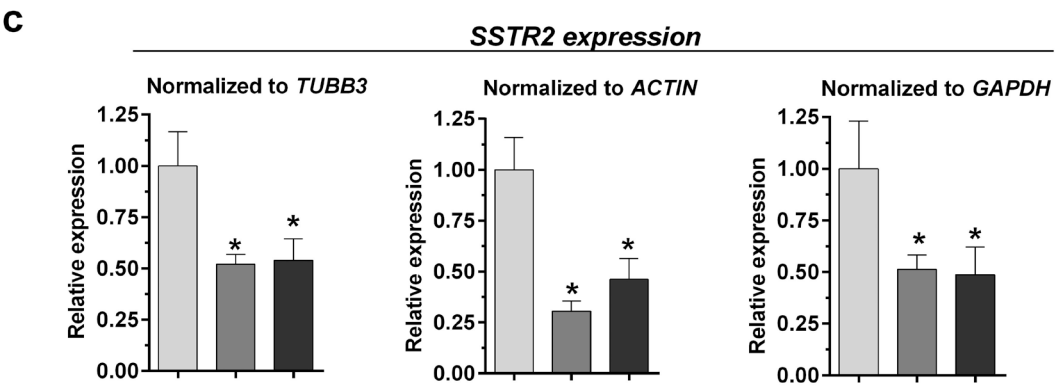

Figure 2

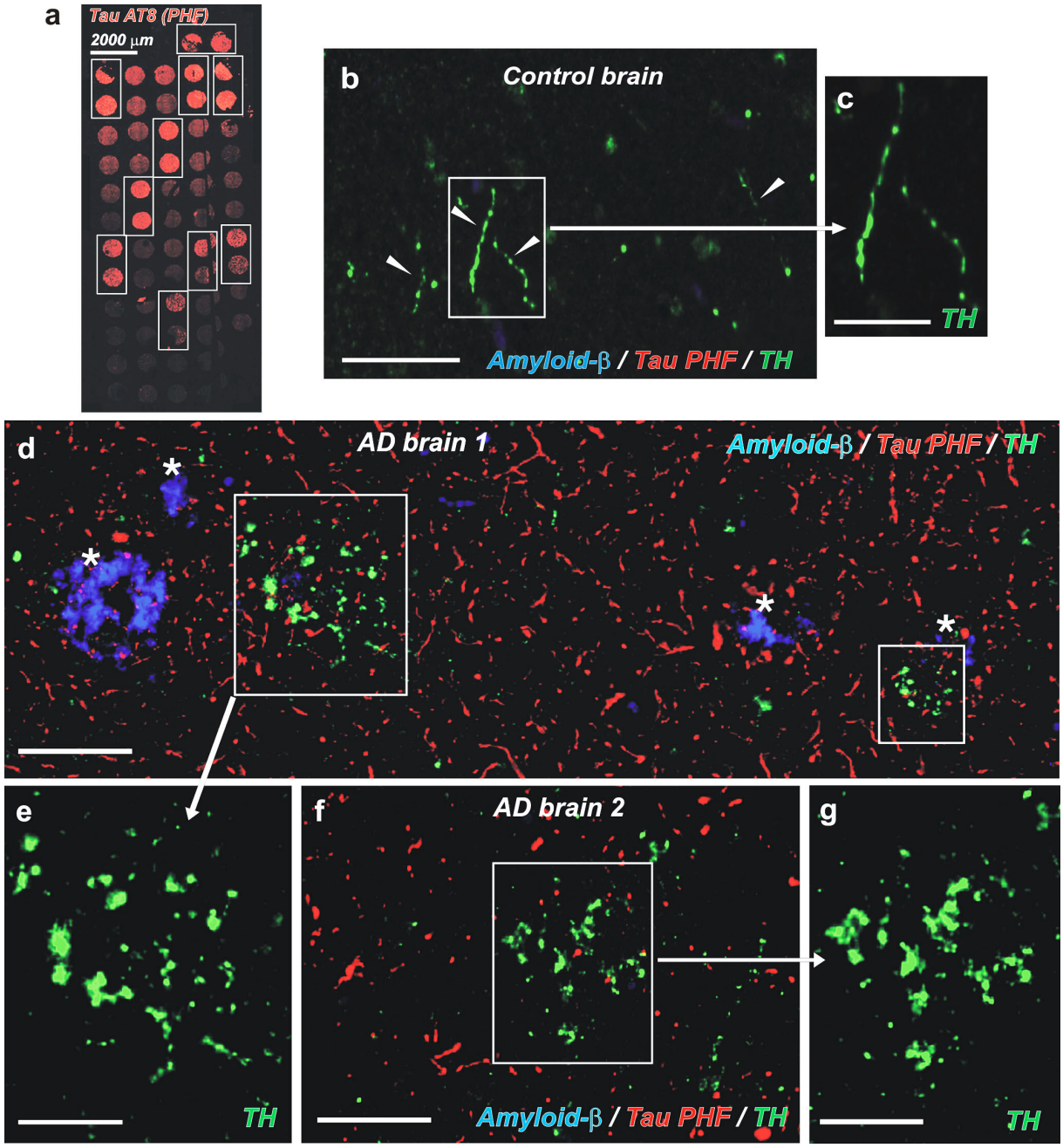
a
Tau AT8 (PHF)
2000 μm
b
Control brain
Amyloid-β / Tau PHF / TH
c
TH
d
AD brain 1
Amyloid-β / Tau PHF / TH
e
TH
f
AD brain 2
Amyloid-β / Tau PHF / TH
g
TH

Figure 3

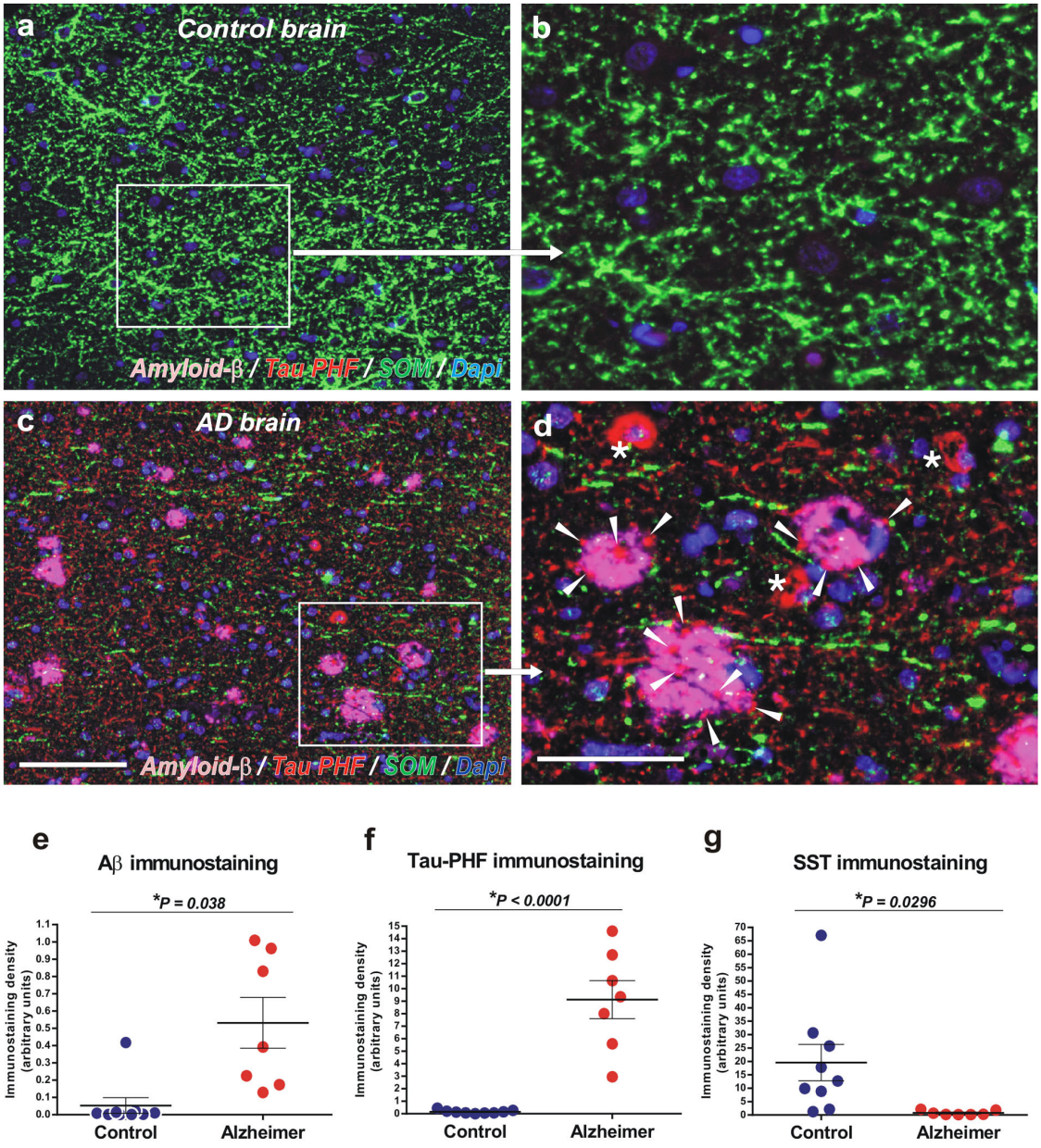
a
Control brain
Amyloid-β / Tau PHF / SOM / Dapi
b
c
AD brain
Amyloid-β / Tau PHF / SOM / Dapi
d
e
Aβ immunostaining
*P = 0.038
Immunostaining density (arbitrary units)
Control
Alzheimer
f
Tau-PHF immunostaining
*P < 0.0001
Immunostaining density (arbitrary units)
Control
Alzheimer
g
SST immunostaining
*P = 0.0296
Immunostaining density (arbitrary units)
Control
Alzheimer

Figure 4

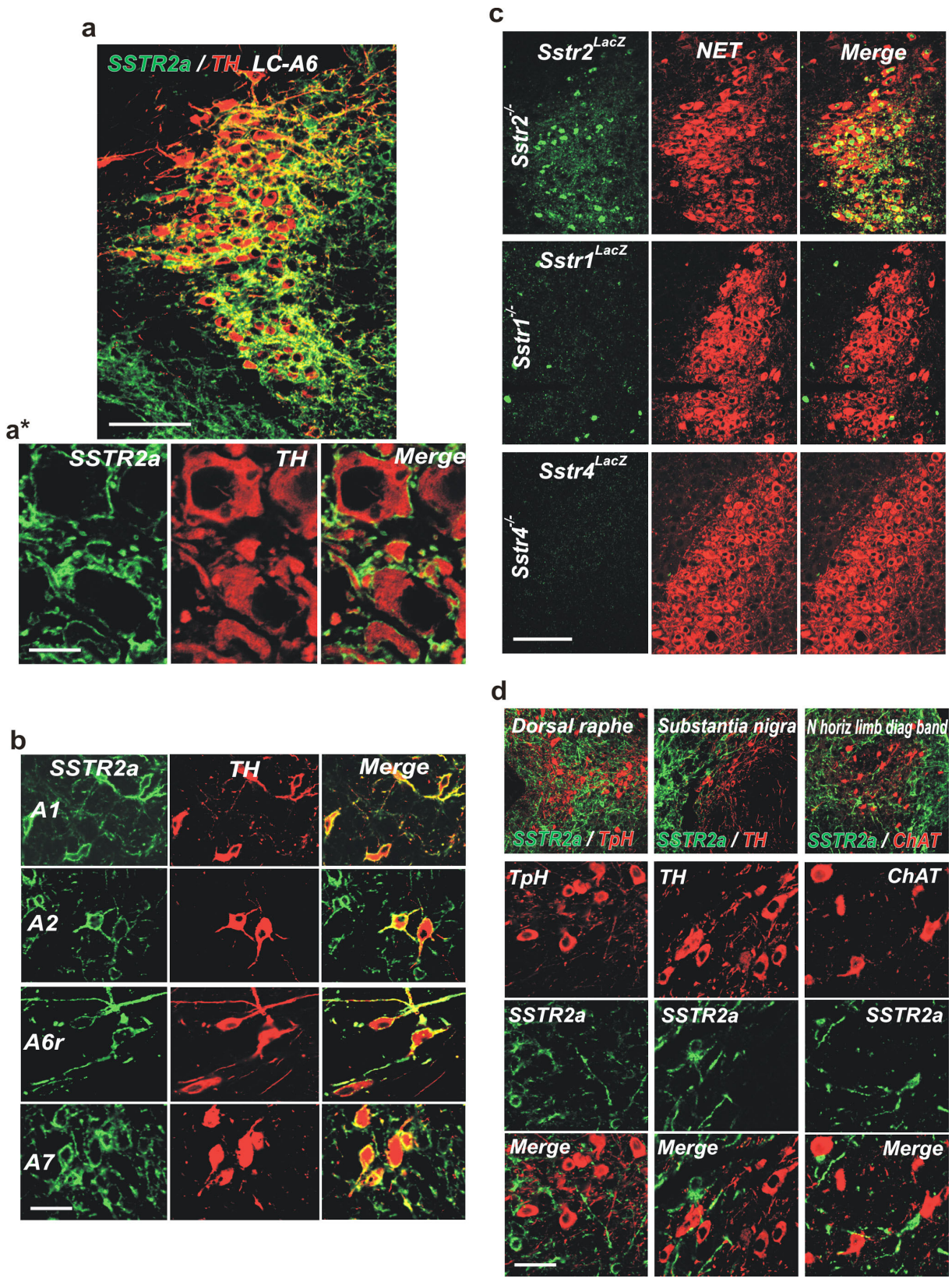
a
SSTR2a / TH LC-A6
a*
SSTR2a
TH
Merge
b
SSTR2a
TH
Merge
A1
A2
A6r
A7
c
Sstr2LacZ
NET
Merge
Sstr2-/-
Sstr1LacZ
Sstr1-/-
Sstr4LacZ
Sstr4-/-
d
Dorsal raphe
Substantia nigra
N horiz limb diag band
SSTR2a / TpH
SSTR2a / TH
SSTR2a / ChAT
TpH
TH
ChAT
SSTR2a
SSTR2a
SSTR2a
Merge
Merge
Merge

Figure 5

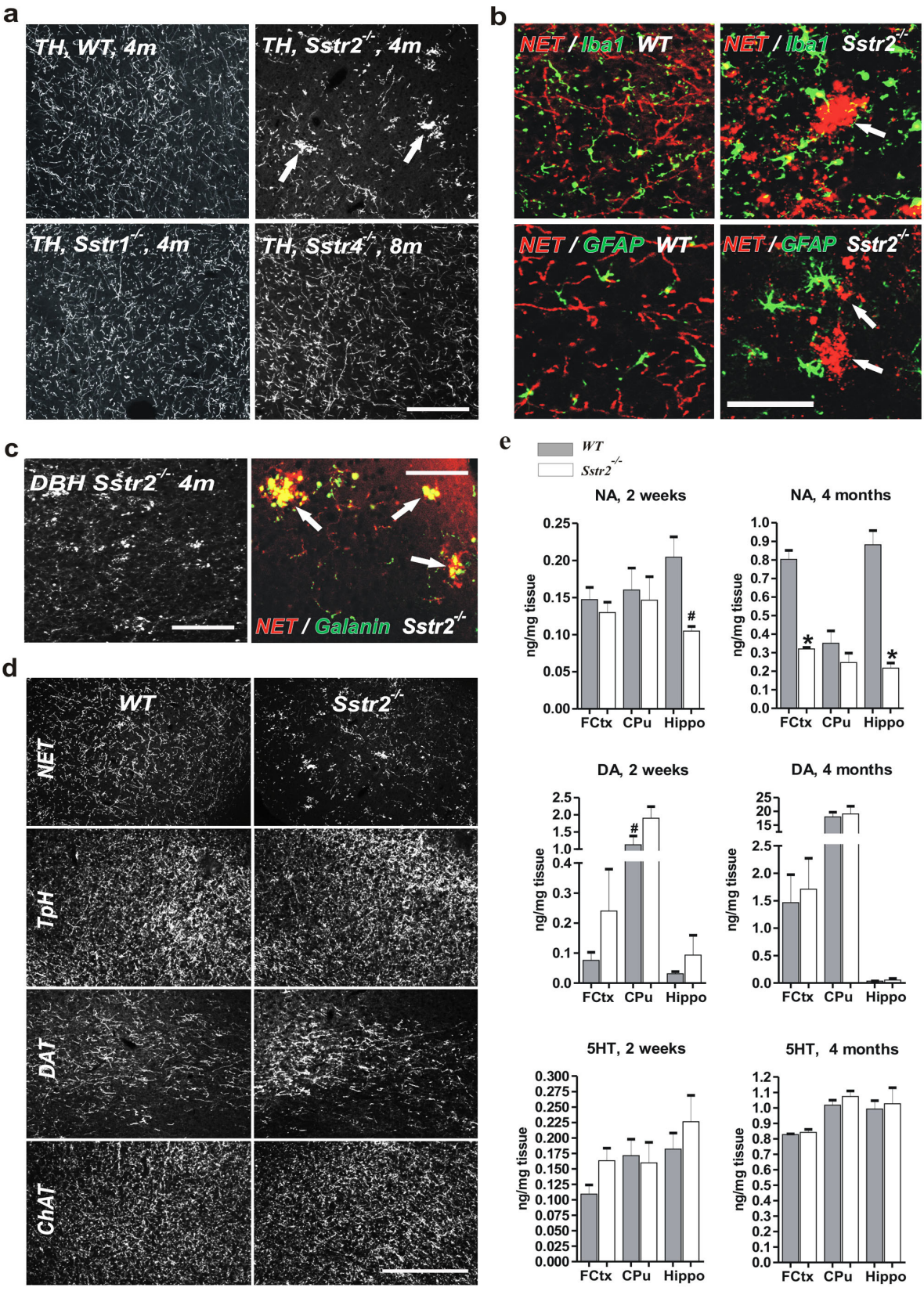
a
TH, WT, 4m
TH, Sstr2-/-, 4m
TH, Sstr1-/-, 4m
TH, Sstr4-/-, 8m
b
NET / Iba1 WT
NET / Iba1 Sstr2-/-
NET / GFAP WT
NET / GFAP Sstr2-/-
c
DBH Sstr2-/- 4m
NET / Galanin Sstr2-/-
d
WT
Sstr2-/-
NET
TpH
DAT
ChAT
e
WT
Sstr2-/-
NA, 2 weeks
NA, 4 months
DA, 2 weeks
DA, 4 months
5HT, 2 weeks
5HT, 4 months
ng/mg tissue
FCtx
CPu
Hippo

Figure 6

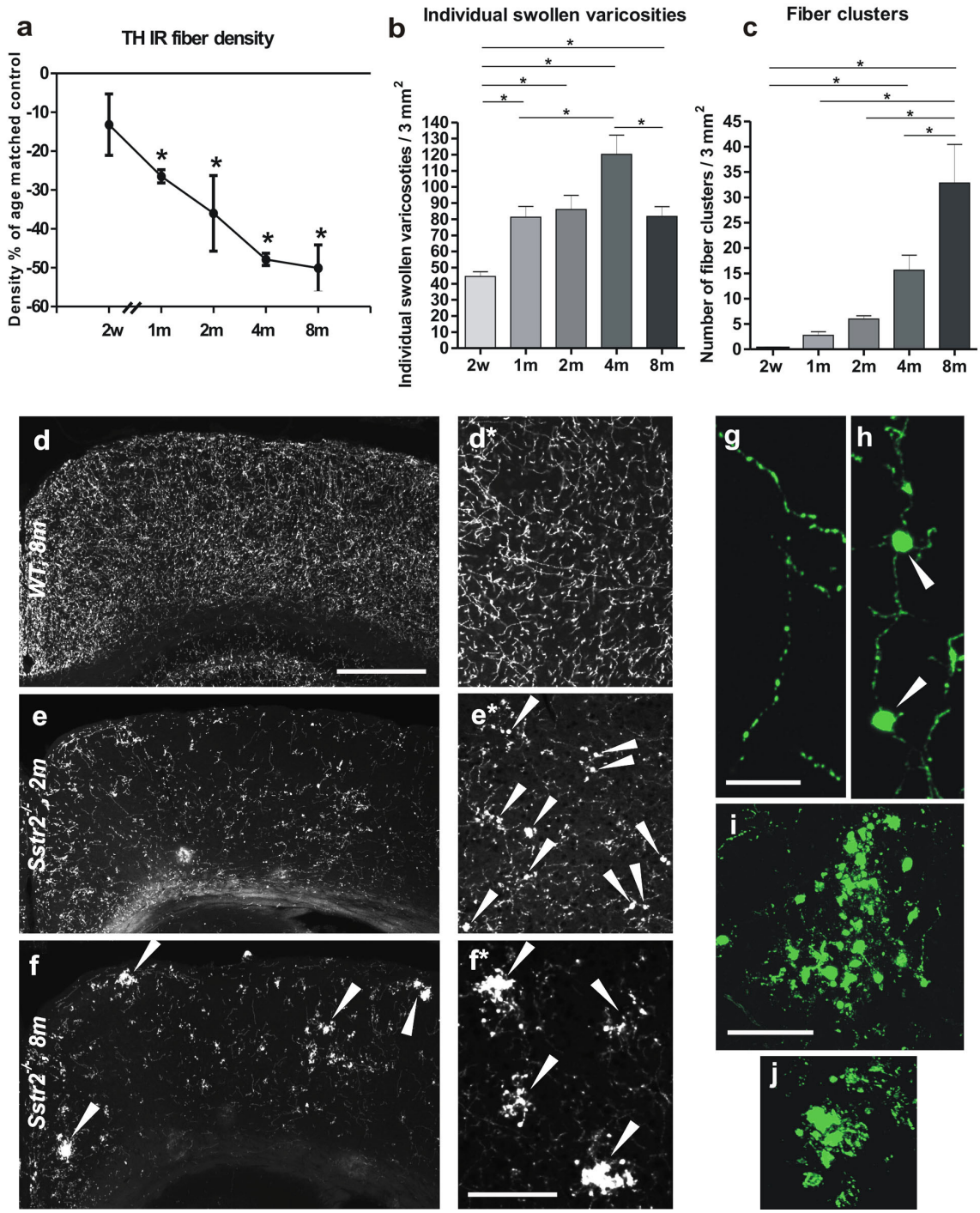
a
TH IR fiber density
Density % of age matched control
0
-10
-20
-30
-40
-50
-60
2w
1m
2m
4m
8m
b
Individual swollen varicosities
Individual swollen varicosoties / 3 mm2
140
130
120
110
100
90
80
70
60
50
40
30
20
10
0
2w
1m
2m
4m
8m
c
Fiber clusters
Number of fiber clusters / 3 mm2
45
40
35
30
25
20
15
10
5
0
2w
1m
2m
4m
8m
d
WT, 8m
d*
e
Sstr2-/-, 2m
e*
f
Sstr2-/-, 8m
f*
g
h
i
j

Figure 7

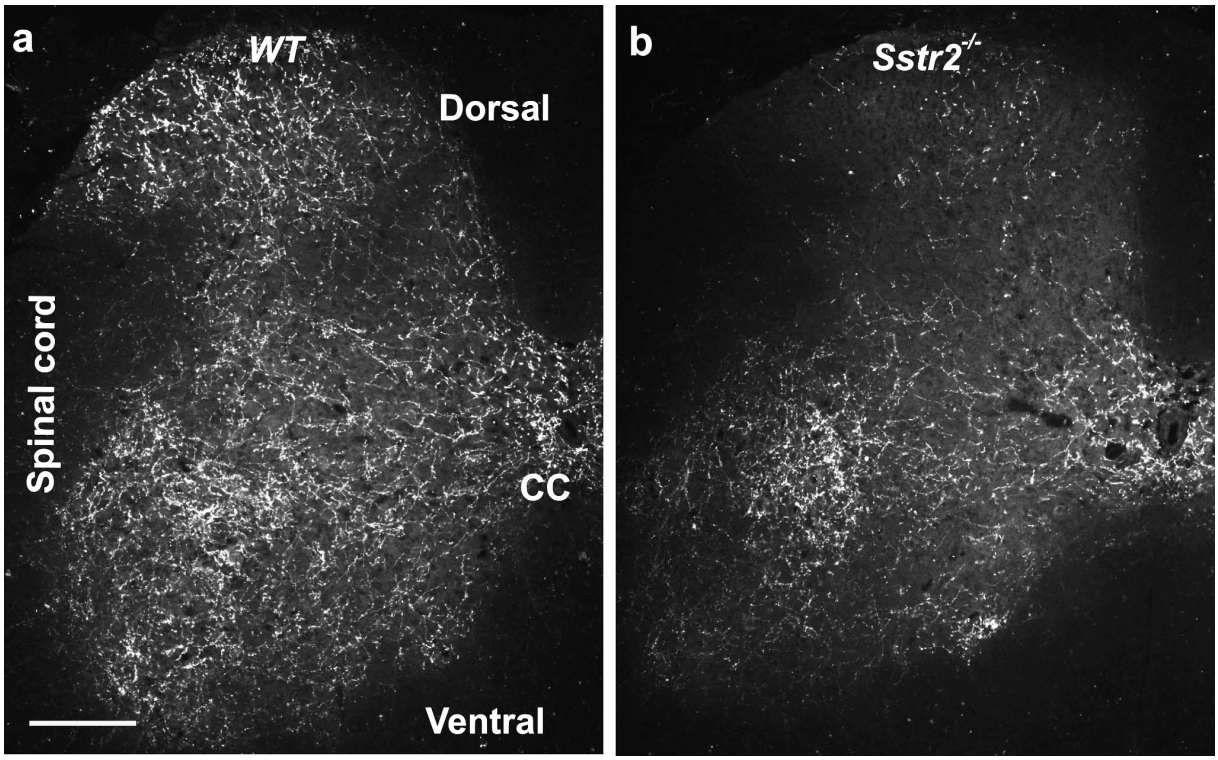

Figure 8

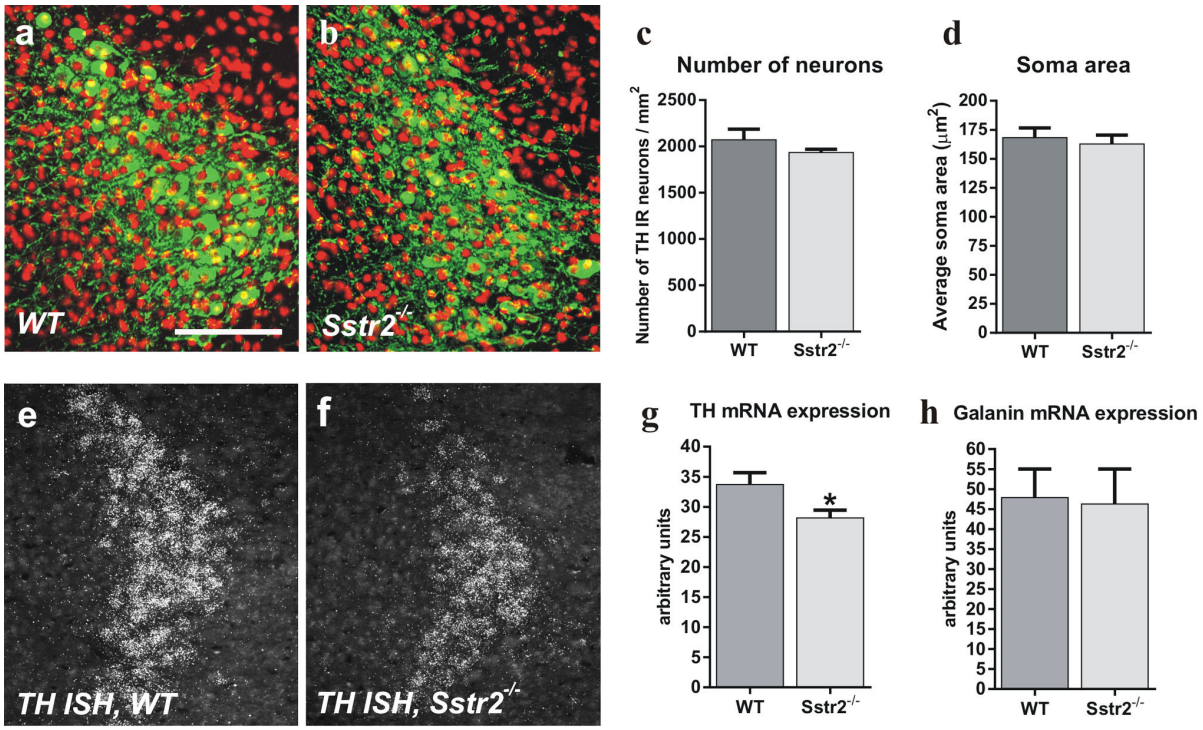
a
WT
b
Sstr2-/-
c
Number of neurons
Number of TH IR neurons / mm2
2500
2000
1500
1000
500
0
WT
Sstr2-/-
d
Soma area
Average soma area (μm2)
200
175
150
125
100
75
50
25
0
WT
Sstr2-/-
e
TH ISH, WT
f
TH ISH, Sstr2-/-
g
TH mRNA expression
arbitrary units
40
35
30
25
20
15
10
5
0
*
WT
Sstr2-/-
h
Galanin mRNA expression
arbitrary units
60
55
50
45
40
35
30
25
20
15
10
5
0
WT
Sstr2-/-

Figure 9

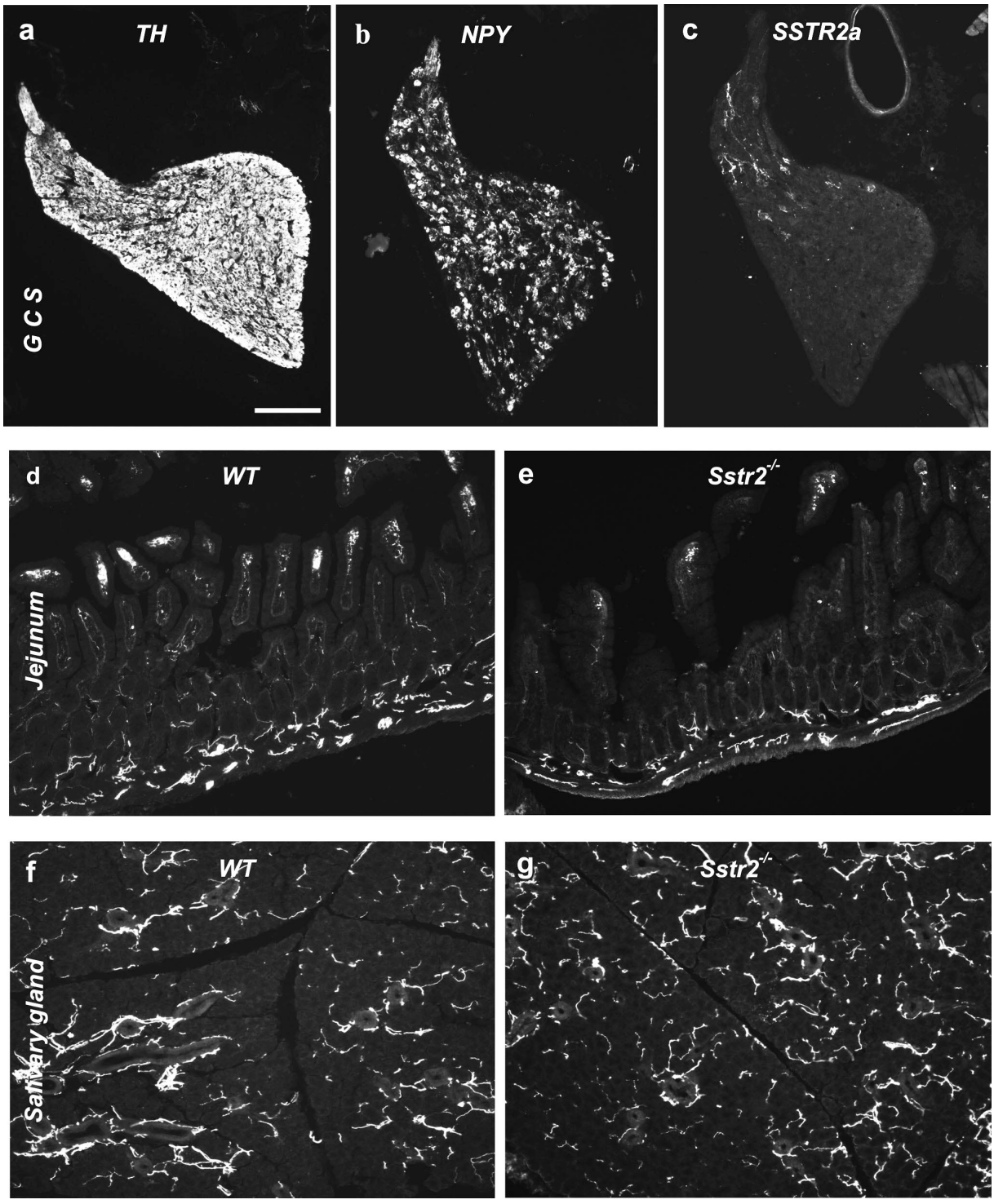
a
TH
G C S
b
NPY
c
SSTR2a
d
WT
Jejunum
e
Sstr2-/-
f
WT
Salivary gland
g
Sstr2-/-

Figure 10

Brain region	nucleus/subregion	4 months (N = 3)	8 months (N = 3)
Bulbus		+	+ - ++
Cerebral cortex	prefrontal Ctx (dorsal peduncular, infralimbic)	++	+++
	cingulate ctx 1-2	++	+++
	motor ctx 1-2.	++	+++
	primary somatosensory ctx 1.	++	++
	primary somatosensory ctx – barrel/upper lip region & secondary somatosensory ctx	++	++ - +++
	agranular insular – disgranular ctx	++ - +++	+++
	piriform ctx	+ - ++	++
	retrosplenial ctx	+ - ++	+++
	visual ctx	++	++
	auditory ctx	++	++
	entorhinal ctx	++	+++
	caudomedial entorhinal ctx	++	+++
Septal region		+	+
Thalamus	anteroventral thalamic nucleus	++ - +++	+++
	ventral thalamic nuclei	++	+++
	nuclei geniculatae	+	++
Hypothalamus	preoptic region	++	+ - ++
	anterior hypothalamus	+	+ - ++
	ventromedial hypothalamic nucleus	+	0 - +
	dorsomedial hypothalamic nucleus	+	+
	perifornical lateral hypothalamus	+	+
Amygdala	basal amygdala	++ - +++	+++
Hippocampus	rostral hippocampus	++	++ - +++
	dorsal hippocampus	++	++ - +++
	ventral hippocampus	++	+++
	area amygdalahippocampalis	++	+++
Brainstem	periaqueductal gray matter	+	+ - ++
	dorsal raphe	0 - +	+
	colliculus inferior	+	++
	locus coeruleus dendrites	0	0

Table 1 Semiquantitative score of degenerative fiber processes in *Sstr2*$^{-/-}$ mice. The score is based on NET (noradrenaline transporter) immunohistochemistry (average of scores obtained from 4-month-old (N = 3) and 8-month-old (N = 3) *Sstr2*$^{-/-}$ mice brains. 0 = no apparent sign of degeneration; + = no cluster, few individual swollen varicosities; ++ = few clusters, many individual swollen neurites; +++ = many clusters, many individual swollen neurites. The descriptions of 'fiber cluster' and 'individual swollen neurite' are provided in the Results (Figure 6, Figure S3, legends).